Simulation of a fully coupled 3D GIA - ice-sheet model for the Antarctic Ice Sheet over a glacial cycle.

Caroline J. van Calcar[1,2], Roderik S.W. van de Wal[2,3], Bas Blank[1], Bas de Boer[4], Wouter van der Wal[1,5]

[1]Faculty of Aerospace Engineering, Delft University of Technology, Delft, 2629 HS, The Netherlands
5 [2]Institute for Marine and Atmospheric research Utrecht, Utrecht University, Utrecht, 3508 TA, The Netherlands
[3]Department of Physical Geography, Utrecht University, Utrecht, 3584 CB, The Netherlands
[4]Earth and Climate Cluster, Faculty of Science, Vrije Universiteit Amsterdam, Amsterdam, 1081 HV, The Netherlands
[5]Faculty of Civil Engineering and Geosciences, Delft University of Technology, Delft, 2628 CN, The Netherlands

Correspondence to: Caroline van Calcar (c.j.vancalcar@tudelft.nl)

10 **Abstract**

Glacial Isostatic Adjustment (GIA) has a stabilizing effect on the evolution of the Antarctic Ice Sheet by reducing the grounding line migration following ice melt. The timescale and strength of this feedback depends on the spatially varying viscosity of the Earth's mantle. Most studies assume a relatively long laterally homogenous response time of the bedrock. However, the mantle viscosity is spatially variable with a high mantle viscosity beneath East Antarctica, and a low mantle viscosity beneath West

15 Antarctica. For this study, we have developed a new method to couple a 3D GIA model and an ice-sheet model to study the interaction between the Solid Earth and the Antarctic Ice Sheet during the last glacial cycle. In this method, the ice sheet model and GIA model exchange ice thickness and bedrock elevation during a fully coupled transient experiment. The feedback effect is taken into account with a high temporal resolution where the coupling time steps between the ice-sheet and GIA model are 5000 yr over the glaciation phase and vary between 500 and 1000 yr over the deglaciation phase of the last glacial cycle.

20 During each coupling time step, the bedrock elevation is adjusted every ice-sheet model time step and the deformation is computed for a linearly changing ice load. We applied the method using the ice-sheet model ANICE and a 3D GIA finite element model. We used results from a regional seismic model for Antarctica embedded in the global seismic model SMEAN2 to determine the patterns in the mantle viscosity. The results of simulations over the Last Glacial Cycle show that differences in mantle viscosity of an order of magnitude can lead to differences in grounding line position up to 700 km and to differences

25 in ice thickness in the order of 2 km at present day near the Ross Embayment. These results underline and quantify the importance of including local GIA feedback effects in ice-sheet models when simulating the Antarctic Ice Sheet evolution over the Last Glacial Cycle.

1 Introduction

The stability of the Antarctic Ice Sheet (AIS) is largely controlled by the bedrock profile (Pattyn & Morlighem, 2020). The

30 bedrock elevation and slope vary in time due to Glacial Isostatic Adjustment (GIA), which is the response of the solid Earth to a changing ice load. Accurate GIA simulations are needed when analyzing the past and future ice sheet dynamics and

stability (e.g. Pan et al., 2021; Gomez et al., 2010). At present, the AIS loses mass in areas where the basal melt increases and the grounding line retreats (Meredith et al. 2019). Fig. 1 shows schematically how GIA affects grounding line migration when the ice sheet retreats. Initially, before the on-set of ice shelf melting, the ice sheet and bedrock topography are represented by

35 the solid grey and brown lines, respectively. The initial position of the grounding line is indicated by p1. Thinning of the ice shelves by increased basal melting, represented by the dashed grey line, leads to a retreat of the grounding line to position p2. Due to a decreasing ice thickness, and thus a decreasing ice load, the Earth's surface experiences a direct instantaneous elastic uplift and a delayed uplift of the viscoelastic mantle of the Earth, represented by the dashed brown line. The uplift of the bedrock causes a local shoaling of water, decreased ice flux towards the ice shelf, and an outward movement of the grounding

40 line to position p3 (Fig. 1). As a consequence, the GIA feedback slows down retreat of the grounding line and acts as a negative feedback (Larour et al., 2019; Konrad et al., 2015; Adhikari et al., 2014; Gomez et al., 2012).
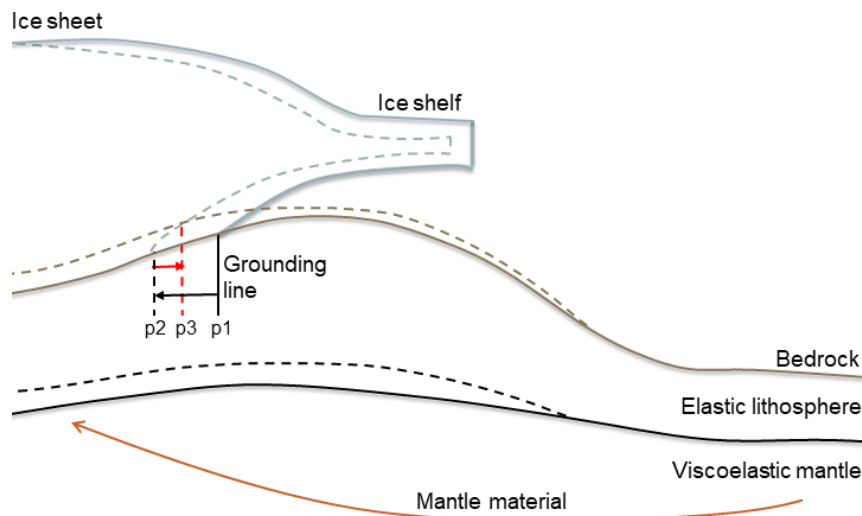
Figure 1: Schematic figure of GIA feedback on grounding line migration. The solid light grey and brown lines represent the initial ice sheet/shelf and bedrock topography respectively before retreat of the grounding line. The solid black line separates the elastic
45 **lithosphere and the viscoelastic mantle. p1 is the grounding line position corresponding to the initial steady state. The dashed light grey line represents the ice sheet/shelf after retreat, the dashed black line is the perturbed mantle elevation, and the dashed brown is the new bedrock surface. p2 is the grounding line position after retreat without GIA effects. P3 is the grounding line position after the GIA response. The change in sea level is not applied as load on the GIA model and only the global mean sea level is prescribed as forcing on the ice-sheet model. The sea level is for this reason not shown in this figure.**

50 There exist other GIA feedbacks on the ice sheet evolution apart from the direct effect on the grounding line via the bedrock elevation. First, the local sea level decreases due to the diminishing gravitational attraction of the ice on the surrounding water in case the ice sheet melts (e.g. de Boer et al., 2017; Gomez et al., 2015). As a consequence, a decrease in sea level reduces the load of the ocean on the bedrock and in turn enhances uplift from GIA, although to a smaller degree than the loss of grounded ice. Second, GIA could steepen or flatten the bed slope dependent on the local topography. A flattened bed slope

55 decreases the rate of basal sliding and ice deformation and therefore decreases the ice flux and ice velocity towards the shelfs (Adhikari et al., 2014). Finally, GIA stabilizes the ice sheet as it reduces the surface elevation change of the ice sheet caused

by surface melt in a warming climate. The reduced lowering of the surface elevation thereby suppresses melt rates (van den Berg et al., 2008).

60   Several types of models have been developed to include GIA in ice-sheet models. A widely used approach to take changes in bedrock topography into account is by using an Elastic Lithosphere Relaxing Asthenosphere model (ELRA) (Le Meur & Huybrechts, 1996). This is a two-layer model that contains a local elastic layer and an asthenosphere that relaxes with a single constant relaxation time. This simplified model is computationally cheap and provides a first-order estimate of bedrock changes (e.g. Pelletier et al., 2022; de Boer et al., 2017; Pattyn, 2017). However, the ELRA approach assumes a radially and

65   laterally homogeneous flat Earth while the actual Earth properties vary spatially. To partly overcome these limitations, Coulon et al. (2021) included regions with different relaxation times in the ELRA model to capture the main patterns of spatial variability in the relaxation time scale. Still, ELRA neglects the effect of self-gravitation, the size dependency of the Earth's response to ice loading, and the fact that larger ice sheets respond to deeper Earth characteristics and smaller ice sheets respond to shallower Earth characteristics (Wu and Peltier, 1982).

70

The solid earth response is mainly determined by the thickness of the elastic lithosphere and the viscosity of the mantle. ELRA models have been improved by coupling the lithosphere with a viscous half-space, where mantle viscosity can be used as input parameter instead of the relaxation time (Albrecht et al., 2020; Bueler et al., 2007). Another approach to compute GIA is self-gravitating visco-elastic (SGVE) spherical Earth models. They compute the response to global ice sheet thickness changes

75   with radially varying Earth models, labeled 1D GIA models, that account for gravity field perturbations . Most 1D GIA studies also account for relative sea level change by solving the sea level equation (DeConto et al., 2021; Pollard et al., 2017; Konrad et al., 2015; de Boer et al., 2014; Nield et al., 2014; Gomez et al., 2013; Whitehouse et al., 2012). For Antarctica, these 1D GIA models commonly use an Earth structure with a strong upper mantle viscosity of 10^{20}-10^{21} Pa·s and a lithosphere of ~100 km thick which is close to the Antarctic average (Gomez et al., 2018; Geruo et al., 2013). The present-day ice surface elevation

80   resulting from a coupled 1D GIA – ice-sheet model with a mantle viscosity of 10^{21} Pa s can be achieved with reasonable accuracy by the ELRA approach with a relaxation time of 3000 yr, but deformation through time differs and it is not known how well other viscosities can be approximated (Pollard et al., 2017; van den Berg et al., 2008; Le Meur & Huybrechts, 1996).

However, even 1D GIA models are oversimplified for realistic Antarctic conditions, as it can be derived from seismic data

85   that the viscosity of the mantle under the AIS varies laterally with six orders of magnitude with much lower viscosities ~10^{18} Pa·s in West Antarctica than the generally assumed global average mantle viscosity (Hay et al., 2017; van der Wal et al., 2015; Ivins et al. 2021). In these low viscosity regions, the Earth's mantle approaches isostatic equilibrium one to two orders of magnitude faster than the timescale of 3000 yr that is commonly used in the application of ELRA models (Whitehouse et al., 2019; Barletta et al., 2018). This can only be overcome by 3D GIA models which have been developed to simulate GIA using

90   a lateral variable rheology in Antarctica (Yousefi et al., 2022; Blank et al., 2021; Powell et al. 2021; Nield et al., 2018; Hay et

al., 2017; van der Wal et al., 2015; A et al., 2013; Geruo et al., 2013; Kaufmann et al., 2005), but those approaches so far neglected the GIA feedback on the ice sheet evolution because they use a predefined ice sheet history.

Whitehouse et al. (2018) emphasize the importance of coupled 3D GIA – ice-sheet models to study regions with a low mantle viscosity and there are ongoing efforts to develop an efficient coupling method on a high temporal resolution using a 1D GIA model (Han et al., 2021). Coupled GIA – ice-sheet models need an iterative method to include the GIA feedback since ice-sheet models need bedrock deformation as input to compute the ice thickness and GIA models need ice thickness as input. We define a coupling time step as the time period over which the ice sheet model and GIA model exchange ice thickness and bedrock elevation during a fully coupled transient experiment. There are coupled 1D GIA – ice-sheet models that use short coupling time steps of tens of years but those models simulate projections and hence consider a much shorter time scale than the glacial cycle (DeConto et al., 2021; Konrad et al., 2015). The only model that couples 3D GIA with ice dynamics is developed by Gomez et al. (2018), who show significant differences in ice thickness of up to 1 km in the Antarctic Peninsula and the Ross Embayment when a 3D Earth rheology was used instead of a 1D rheology. From this model it can be concluded that uplift is typically underestimated in West Antarctica and overestimated in East Antarctica when using lateral homogenous Earth structures in ELRA or 1D GIA models (Nield et al., 2018). Gomez et al. (2018) applies the following iteration method to simulate the AIS evolution from 40 kyr to present-day. First, the 3D GIA model computes bedrock elevation changes relative to the geoid at time steps of 200 yr for the entire 40 kyr using ice thickness changes from a previous coupled 1D GIA simulation. These bedrock elevation changes are corrected at each time step for the difference between the simulated present-day bedrock topography and the observed present-day topography. The corrected bedrock elevation changes are passed to the ice-sheet model to recompute the ice thickness history for the entire period of 40 kyr till present-day with time steps of 200 yr. Finally, the new ice thickness history is passed to the 3D GIA model and the process is repeated until the ice and bedrock elevation histories converge. Typically, only four iterations are needed. However, both models are still simulated over the entire period of 40 kyr with a fixed ice or bedrock elevation history as input. As a consequence the coupling time step between ice sheet model and 3D GIA model is 40 kyr. Yet, for example in the Amundsen Sea embayment in West Antarctica, GIA occurs on decadal to centennial timescales (Barletta et al., 2018). Present-day GIA estimations and the evolution of the ice sheet could therefore be improved by including the 3D GIA feedback in a coupled model at coupling time steps shorter than 40 kyr.

This study presents a method to fully couple an ice-sheet model and a 3D GIA model on century to millennial timescales from 120 ka onwards. The method simulates the 3D GIA feedback by iterating an ice-sheet model and a 3D GIA model at every single coupling time step. The method is applied using the ice-sheet model ANICE (de Boer et al. 2013), and a 3D GIA finite element (FE) model (Blank et al., 2021), where the coupling time steps are 5000 yr over the glaciation phase and vary between 500 and 1000 yr over the deglaciation phase of the last glacial cycle. The GIA model computes deformation due to ice loading and does not solve the sea level equation, but the viscoelastic model does account for the effect of self-gravitation of the mantle deformation when a 1D Earth structure is used. To decrease computational time, the GIA model excludes the effect of self-

125   gravitation when a 3D Earth structure is used which is explained in section 2.2. Global mean sea level (GMSL) from the northern hemisphere ice-sheets is prescribed in the ice-sheet model. The ice-sheet model is applied to Antarctica to assess the impact of the stabilizing GIA effect on the AIS evolution over the last glacial cycle using 1D and 3D Earth structures.

    We assess whether widely used 1D Earth structures, for example those used by Pollard et al. (2017), yield similar stability
130   characteristics for ice sheet evolution caused by bedrock uplift, in comparison to 3D Earth structures during the deglaciation phase. The developed coupled model can be applied to different regions and the coupling method could be applied to different ice-sheet models and GIA models. The model has potential to improve GIA estimates, and hence corrections for ongoing GIA to geodetic data (e.g. Scheinert et al., 2021; Shepherd et al., 2018). This method cannot only be applied to improve glacial-interglacial ice sheet histories, but also for projections of the AIS evolution.

135 **2 Method**

    The coupling method that we present in this paper can be applied to any ice-sheet and GIA model, as long as the models have the possibility to restart at certain time steps. We applied the coupling method to the ice sheet model ANICE and the 3D GIA model, which are introduced first in this section 2.1 and 2.2. The coupling method alternates between the ice-sheet model and the GIA model, where the ice-sheet model uses the bedrock deformation computed by the GIA model and the GIA model uses
140   the changes in ice thickness computed by the ice-sheet model. The interpolations that are necessary to feed the ice-sheet model output to the GIA model and the GIA model output to the ice-sheet model are discussed in the supplementary material on page 5. Finally, we describe the coupling method in section 2.3. The models are coupled at a coupling time step that varies during a glacial cycle. During the glaciation phase, the coupling time step is 5000 yr and during the deglaciation phase, the coupling time step is 1000 and 500 yr. The effect of the size of the coupling time step is discussed in section 2.3.1. At intermediate time
145   steps the ice-sheet model uses a linear interpolation of the bedrock changes and the GIA model uses a linear interpolation of the ice thickness changes.

2.1 Ice-sheet model: ANICE

    The ice-sheet model ANICE is a global 3D ice-sheet model allowing to simulate the AIS, Greenland ice sheet, Eurasian ice sheet and North American ice sheet separately or simultaneously (de Boer et al., 2013). Each ice sheet can be simulated on
150   different equidistant grids. The horizontal resolution is 20 km for Greenland and 40 km for the other regions. The temporal resolution of ANICE is 1 yr, hereafter referred to as the ANICE time step. ANICE has been used for a variety of experiments (Berends et al., 2019; Berends et al., 2018; Bradley et al., 2018, de Boer et al., 2017; Maris et al., 2014; de Boer et al., 2013). For this study, ANICE is used to simulate the Antarctic ice sheet evolution with a resolution of 40x40 km. Atmospheric temperature and GMSL act as the main forcing for the ice-sheet model, as is shown in Fig. S.1, and are the result of previous

155   ice volume reconstructions using ANICE and benthic isotopes forcing (de Boer et al., 2011). The accumulation for the ice sheet is computed using present-day monthly precipitation from ERA40, which are temporally extrapolated as a function of the free atmospheric temperature (Bintanja et al., 2005; Bintanja & van de Wal, 2008). A time and latitude dependent surface temperature-albedo-insolation parameterization is used to calculate ablation (Berends et al. 2018). Insolation changes are based on the solution by Laskar et al. (2004). The Shallow Shelf Approximation (SSA) (Bueler and Brown, 2009) is used to solve

160   mechanical equations to determine sliding and velocities of ice shelves, and the Shallow Ice Approximation (SIA) is used to compute velocities of grounded ice (Morland, 1987; Morland & Johnson, 1980). Basal sliding follows a Weertman friction law where friction is controlled by bed elevation. The position of the grounding line and GMSL determine whether ice is grounded or floating, thus whether the ice experiences sub-shelf melt or not. A combination of the glacial-interglacial parametrization by Pollard and DeConto (2009) to scale the global mean ocean temperature beneath the shelf, and the ocean

165   temperature-based formulation by Martin et al. (2011) are used to compute sub-shelf melt. This parametrization assumes a linear relation between sub-shelf melt and ocean temperature. Changes in ocean circulation are not taken into account.

Besides the effect of GMSL, there is an effect from regional sea-level variations as well. Although the effect of the northern hemisphere ice sheets on GMSL is significant, the effect of the AIS itself is most important for regional sea level (Gomez et

170   al., 2020). At regions where grounded ice melts, such as the Ross and the Filchner-Ronne embayments during the deglaciation phase, the near field sea level is reduced due to the decreasing gravitational attraction between the ice sheet and the ocean. De Boer et al. (2014) studied the differences between using ANICE with a gravitationally self-consistent sea-level, and with global mean sea level. At last glacial maximum, the ice volume of the AIS is lower when including regional sea level because the increased regional sea level due to increased gravitational attraction of the growing ice sheet leads to a small reduction in

175   grounded ice. During the deglaciation, the differences in ice volume are small. The spatial variation caused by Northern Hemisphere ice volume changes over a glacial cycle is smaller than the spatial variation in regional sea level by Antarctic changes and is therefore considered a second order effect. The regional sea level variation is not yet included in this model.

The standard version of ANICE uses the ELRA method to compute bedrock elevation changes using a uniform relaxation time

180   that is usually taken to be 3000 yr. For this study, ANICE is adjusted to use the bedrock deformation computed by a GIA model instead of computing the bedrock deformation using the ELRA method (see section 2.3.1 for explanation of the chosen coupling time steps). The initial topography at 120 ka is taken from ALBMAP (Le Brocq et al., 2010). Within one coupling time step, the bedrock elevation is updated in ANICE at time steps of 1 yr using linear interpolation of the deformation computed by the GIA model:

185    $b_t = b_{t0} + \frac{db}{\Delta t_{coupling}} \cdot \Delta t_{ANICE}$,   (1)

where b_t refers to the updated bedrock elevation at the ANICE time step, b_{t0} refers to the bedrock elevation at the beginning of the coupling time step, $\frac{db}{\Delta t_{coupling}}$ refers to the total deformation of one coupling time step computed by the GIA model divided

by the length of the coupling time step in years, and Δt_{ANICE} refers to the ANICE time step of 1 yr. Linear interpolation introduces inaccuracy of the true GIA deformation which generally follows an exponential curve. As a consequence, the total

190   deformation at the end of the coupling time step is the same, but the deformation would be slightly underestimated at the beginning of the coupling time step. This effect is higher at regions with a lower viscosity of the Earth's mantle due to the increased nonlinearity of the Earth's response compared to higher viscosity regions. The effect of this approximation can be reduced by reducing the length of the coupling time step as is shown in section 2.3.1.

2.2 GIA model

195   The GIA finite element (FE) model from Blank et al. (2021) is used, which is based on the commercial finite element method (FEM) software ABAQUS (Hibbitt et al., 2016) following Wu (2004). It computes bedrock changes for surface loading on a compressible spherical Earth ($\upsilon = 0.28$) with a composite and Maxwell rheology. The effect of density variations required for full compressibility is not included. Each element of the model gets assigned a dislocation and diffusion parameter from which the mantle viscosity can be computed based on, among others, the applied stress from surface loading. Section 2.2.2 discusses

200   how these parameters, and the viscosity are computed. The FEM approach allows for discretization and computation of stresses and the resulting deformation in the Earth using a modified stiffness equation and Laplace's equation (Wu, 2004). The ice loading is applied to the GIA FE model at each coupling time step. When running the GIA FE model, each coupling time step is divided in increments for numerical integration inside the finite element model. The size of each subsequent increment is determined based on how fast the computation of the deformation converges. In this study, each coupling time step is divided

205   into approximately 30 increments so that the nonlinear solution path can be followed sufficiently accurate. The advantage of this FEM approach based on ABAQUS is its flexibility as its grid size and rheology can be adjusted. Furthermore, FE models operate in the time domain so the program can be stopped at each time step and all information about the state of stress is stored, contrary to SGVE models which operate in the Laplace domain for which the entire ice history has to be available to compute the next time step (e.g. de Boer et al., 2014), introducing complication if the coupled evolution is addressed. Because

210   of the solution in the temporal domain FE models can exchange information with the ice-sheet model at every required time step. This advantage allows, for example, to simulate the glaciation phase of the last glacial cycle once on a high spatial and temporal resolution and to use the state of the Earth at the end of the glaciation phase as a starting point for different experiments of the deglaciation phase where, for example, the coupling step size or the forcing of the ice-sheet model is adjusted. The restart option also allows for simulation of projections where the model is restarted from an initialized GIA FE

215   - ice-sheet model.

The adopted 3D GIA FE model from Blank et al. (2021) used a prescribed ice load history for all time steps in the GIA FE model and iterates several times over the past 120000 yr to include self-gravitation (Wu, 2004). However, restarting with a different ice load at each coupling time step is necessary to include the GIA-feedback on the ice dynamics. For this reason

220   adjustments to the GIA FE model have been made, to be able to continue the GIA FE model with a new ice load after each

coupling time step using the RESTART option in Abaqus. When simulating the 1D Earth structures, two iterations of the GIA FE model are performed over each coupling time step to include self-gravitation before moving on to the next time step. When simulating the 3D Earth structures, only one iteration of the GIA FE model is performed over each coupling time step to decrease the simulation time with 50%. The difference between including and excluding the effect of self-gravitation is less than 10% of the total deformation as shown in Fig. S.2. For future studies, the same iteration over each coupling time step could be used to solve the sea level equation (Wu, 2004; Blank et al., 2021) and rotational feedback (Weerdesteijn et al., 2019).

The applied changes in ice loading are relative to the present-day ice load, as it is assumed that the Earth was in isostatic equilibrium with present-day ice loading at the beginning of the last glacial cycle. The ice load is computed at each time step by computing grounded ice thickness above floatation, taking into account the relative sea level change, as described in Simon et al. (2010). The ice load is computed by ANICE using:

$$H_{AF} = H - \max\left(0, (SL - b) \cdot \frac{\rho_w}{\rho_i}\right) \qquad (2)$$

where H_{AF} refers to the ice thickness above floatation of grounded ice, H to the ice thickness of grounded ice, SL to the sea level relative to present day sea level, b to the bedrock elevation relative to present day sea level, and ρ_w and ρ_i to the density of water and ice respectively. The change in ice load is applied as a linear change on the GIA FE model during each coupling time step. This is an approximation of the true ice dynamics over the coupling time step, of which the ice dynamic equations are solved on much shorter timescales (1 yr) than the coupling time steps and are nonlinear. The determination of the chosen coupling time steps of 5000, 1000 and 500 yr is described in section 2.3.1.

Not only ice loading causes deformation, but also ocean loading due to temporal variations in sea level. We conducted a test where we prescribed a spatially variable global ice and ocean loading caused by other ice mass changes, taken from Whitehouse et al. (2012), in addition to loading from the Antarctic ice-sheet model. From the results of the test, we conclude that the effect of global ocean and ice loading on deformation could be important on the scale of individual glaciers in Antarctica, but the load of global ice and ocean loading from other ice mass changes was negligible compared to the ice load variations on the scale of the AIS. Including global loading in the GIA FE model increases the computation time because a load is applied to every surface element globally instead of only on the surface elements where there is a change in grounded ice in Antarctica. Thus, loading due to other ice masses, spatially variable ocean loading, and loading due to variations in Earth's rotation, are not considered with the aim of reducing computational burden, as this paper focuses on the direct effect of mantle viscosity.

2.2.1 Model setup and resolution

In the GIA model adopted for this study, referred to as the GIA FE model (Blank et al., 2021; Hu et al., 2017), a different mantle viscosity can be assigned to each element which allows for the use of 3D Earth structures (van der Wal et al., 2015). Other parameters (such as density and Youngs modulus) are taken constant in layers that represent the core, lower and upper

mantle and the elastic lithosphere. The horizontal grid has a higher resolution over Antarctica, which is visible in Fig. 2. Sensitivity tests for the grid size are conducted for the trade-off of accuracy versus the computation time. For these tests, the
255   GIA FE model is loaded with a parabolic ice cap for 1000 yr using 4 different spatial resolutions, respectively: 70, 55, 30 and 15 kilometers. The details of the test are described in Fig. S.3 in the supplementary materials. The tests show that using a horizontal resolution of 15 by 15 kilometers instead of 30 by 30 kilometers decreases the deformation with 0.01 percent over 1000 yr and increases the computation time of the GIA FE model by approximately 30 percent to 15 minutes (Fig. S.3). A coarser resolution of 55x55 km does not notably reduce the computation time. Therefore, an resolution of approximately 30
260   by 30 km is chosen at the surface in Antarctica from 62 degrees latitude to the south pole, and 200 by 200 km elsewhere in the GIA FE model. Since the grid lies on a sphere, the elements are not equal, but their size approaches the given resolution. The resolution in the lower mantle and core are double as coarse as the lithosphere and the upper mantle. The chosen resolution results in approximately 300,000 elements divided over several layers, where the lithosphere and upper mantle have double the elements of the lower mantle and the core. The FE model is divided in eight layers for the 1D simulations and nine layers
265   for the 3D simulations to represent the upper and lower mantle so that the elements in each layer lie at the same depth (see Table 1 for detailed parameters of the layers). The bottom of the upper mantle is connected to the lower resolution lower mantle with the use of so-called tie constraints. Fig. 2 shows an example of a change in a deformed sphere due to ice unloading at East Antarctica and ice loading at West Antarctica, with a relatively high-resolution in and around Antarctica and lower resolution in the far-field.
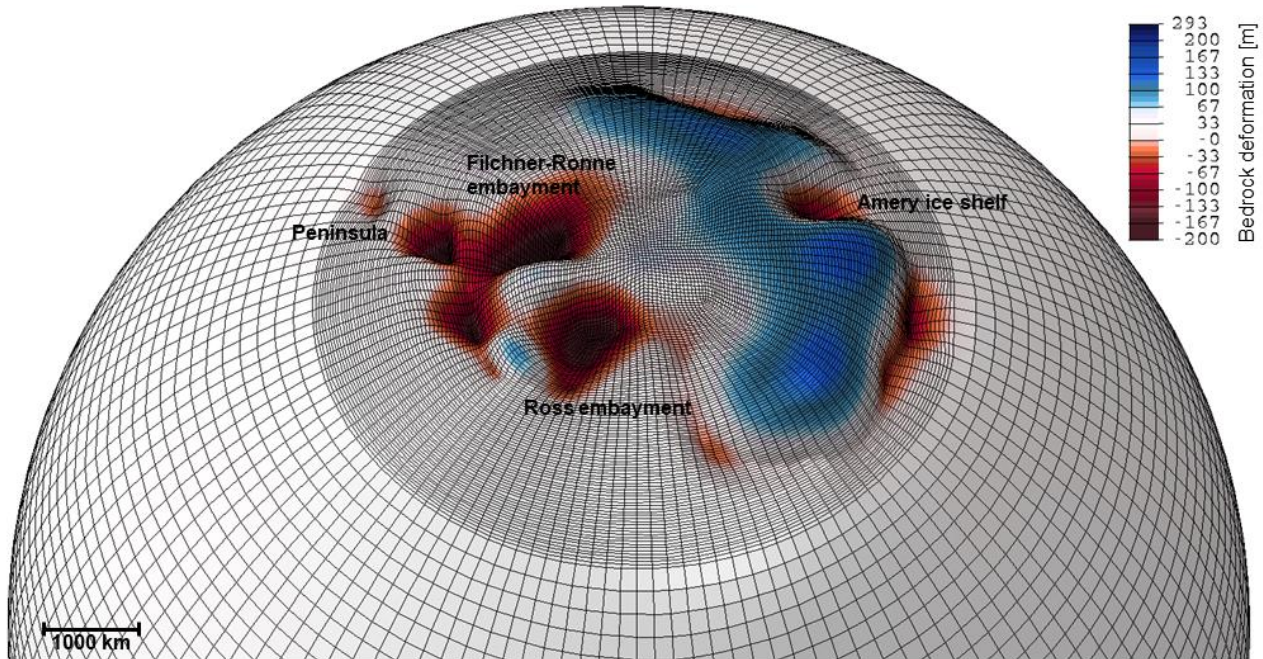
270

Figure 2: Example of the deformed Earth simulated by the GIA FE model at 115 ka. The grid has a higher resolution area of 30 by 30 km at latitudes until -60 degrees, and a lower resolution area of 200 by 200 km above -60 degrees latitude. The ice sheet is mainly growing in West Antarctica, causing subsidence, and slightly decreasing in East Antarctica which causes uplift.

275 Following the 5-layer model used in Spada et al. (2011), one value for density, Young's modulus and, in the case of a 1D model, a viscosity is assigned to each layer, as is shown in Table 1. In case of a 3D Earth structure, the elastic top layer is fixed till 35 km depth as this is the thinnest lithosphere found in West Antarctica (Pappa et al., 2019), and a 3D rheological model with specific dislocation and diffusion creep parameters is assigned to each element between 35 and 670 km depth, as is described in section 2.2.2. The effective lithospheric thickness is therefore spatially variable and follows from the effective

280 mantle viscosity. If the viscosity in a region is so high that viscous deformation in one of the top layers is negligible over the entire cycle, the region can be considered to be part of the lithosphere (e.g. van der Wal et al., 2013; Nield et al., 2018). This will lead to a thicker effective lithosphere than 35 km in most of Antarctica. Thus, the second model layer partly consists of lithosphere and partly of upper mantle and is called the shallow upper mantle in Table 1. In the 1D model, the lithosphere is prescribed as 100 km thick which is similar to the lithospheric thickness used in Gomez et al. (2018). The chosen viscosities

285 of $5\cdot10^{21}$ and 10^{21} Pa·s for the mantle between 420 and 2891 km depth, are shown in Table 1, and consistent with GIA based inferences of radial viscosity (Lau et al., 2016; Lambeck et al., 2014). The core is included in the model only through boundary conditions to provide a buoyancy force on the mantle (Wu et al., 2004). The complete overview of the parameter set up is shown in Table 1.

Table 1: Material properties of the GIA FE model. The top of upper mantle 2 is at 100 km depth for the 1D simulation and at 35 km for the 3D simulation.

Earth layer	Depth [km]	Number of layers in model	Density [kg/m³]	Young's modulus [Pa]	Viscosity [Pa·s]
Top layer	0 - 35$^{(3D)}$/100$^{(1D)}$	1	3037	$0.50605 \cdot 10^{11}$	$1 \cdot 10^{44}$
Upper mantle	35$^{(3D)}$/100$^{(1D)}$ – 420	3/4	3438	$0.70363 \cdot 10^{11}$	1D/3D variable
Transition zone	420 - 670	2	3871	$1.05490 \cdot 10^{11}$	$1 \cdot 10^{21}$
Lower mantle	670 - 2891	2	4978	$2.28340 \cdot 10^{11}$	$5 \cdot 10^{21}$
Core	2891 - 6371	1	10750	$1 \cdot 10^{-20}$	0

2.2.2 Rheology and seismic models

The deformation as a result of the applied ice load depend on the rheological model that is used by the GIA FE model. Rheological models describe the relation between stress and strain. The 1D version of the GIA FE model uses a linear Maxwell rheology at all depths, whereas the 3D version uses a composite rheology following van der Wal et al. (2010) at depths between 30 and 420 km (see Table 1). The composite rheology combines two deformation mechanisms, diffusion and dislocation creep such that the strain computed in ABAQUS is:

$$\Delta\epsilon_{ij} = \frac{3}{2}\left(B_{diff} + B_{disl}\tilde{q}^{n-1}\right)q_{ij}\Delta t, \tag{3}$$

where $\Delta\epsilon_{ij}$ is the strain, B_{diff} and B_{disl} are the spatially variable diffusion and dislocation parameters respectively, $\tilde{q}$ is the Von Mises stress which is assumed to be 0.1 MPa (Ivins et al., 2021), n is the stress exponent, taken to be 3.5, consistent with Hirth and Kohlstedt (2003), q_{ij} is the deviatoric stress tensor, and Δt is a variable time increment for the numerical integration within the coupling time step. The increments are determined automatically depending on the applied stress and the size of the coupling time step. Detailed explanation of the implementation of the composite rheology in the FE model can be found in Blank et al. (2021).

From Eq. 3 it can be derived that the effective viscosity (η_{eff}) for each element of the GIA FE model (van der Wal et al., 2013) becomes:

$$\eta_{eff} = \frac{1}{3B_{diff} + 3B_{disl}q^{n-1}}, \tag{4}$$

The diffusion and dislocation parameters used in this study are derived from the flow law from Hirth and Kohlstedt (2003) and given by Eq. 5a and 5b respectively:

$$B_{diff} = A_{diff}d^{-3}f_{H_2O}^1 e^{-\frac{E+PV}{RT_{x,y}}}, \tag{5a}$$

$$B_{disl} = A_{disl}d^0 f_{H_2O}^{1.2} e^{-\frac{E+PV}{RT_{x,y}}}, \tag{5b}$$

where A is experimentally determined ($A_{diff} = 10^6$ MPa, $A_{disl} = 90$ MPa), d is the grain size, f_{H_2O} is the water content, E is the activation energy, P is the depth dependent pressure (Kearey et al., 2009), V is the activation volume, R is the gas constant

315 and $T_{x,y}$ is the spatially variable absolute temperature. A, E and V are different according to the values for wet and dry olivine. All parameters, except temperature, grain size and water content, are taken from Hirth and Kohlstedt (2003). The temperature is derived from an Antarctic seismic model and a global seismic model for each element of the GIA FE model following approach 3 in Ivins et al. (2021). Following this approach, seismic velocity anomalies are converted to temperature, assuming that all seismic velocity anomalies are caused by temperature variations (Goes et al., 2000). Derivatives of seismic velocity

320 anomalies to temperature anomalies are provided as a function of depth in the mantle (Karato et al., 2008). Antarctic seismic velocity anomalies are taken from Lloyd et al. (2020) and global velocity anomalies for regions above -60 degrees latitude are taken from SMEAN2 which is an average of three seismic models (Becker & Boschi, 2002). The models are combined with a smoothing applied at the boundary at -60 degrees latitude. Mantle melt is assumed to have a relatively small influence on upper mantle viscosity and is therefore not included in this study (van der Wal et al., 2015).

325

Following Eq. 3-5, the mantle viscosity, and thus the deformation, is dependent on the grain size and water content. As little information exists on grain size and water content, these parameters are kept spatially homogeneous (van der Wal et al., 2015). We obtained two different 3D rheologies by choosing a grain size of 4 mm and a water content of 0 (hereafter referred to as 3Ddry) and 500 ppm (hereafter referred to as 3Dwet) to obtain rheologies that can be considered realistic based on other

330 viscosity studies (e.g. Blank et al., 2021; Gomez et al., 2018; Hay et al., 2017). A water content of 500 ppm is within the range of water content found in Antarctic xenoliths (Martin, 2021).

The two rheology models give an idea of some, though not all, variation in 3D mantle viscosity. The viscosity of both 3D rheologies is shown at three depths in the two right columns of Fig. 3 (Fig3c-d, g-h, k-l). Increasing the water content lowers

335 the mantle viscosity but the pattern of viscosity variations is maintained (Karato et al., 1986; Blank et al., 2021). This can be seen in Fig. 3, where the mantle viscosity of 3Ddry is approximately one order of magnitude higher than the mantle viscosity of 3Dwet. Both 3D rheologies provide an upper mantle viscosity of approximately 10^{18} Pa·s in West Antarctica, which is comparable with Barletta et al., (2018), who estimated such low viscosities in West Antarctica by constraining the GIA model using GPS and seismic measurements, and with Blank et al. (2021), who confirmed that a mantle viscosity of $10^{18\text{-}19}$ Pa·s is

340 plausible in the Amundsen Sea sector, based on the WINTERC 3.2 temperature model which is constrained by seismic data and satellite gravity data (Fullea et al., 2021). The viscosity pattern of both 3D rheologies used in this study, and the viscosity value of the 3Ddry rheology, are similar to the mantle viscosity used by Gomez et al. (2018) and Hay et al. (2017), who infer mantle viscosity by scaling seismic anomalies to viscosity anomalies and adding them to background viscosity profile from GIA or geodynamic studies. A background viscosity can be inferred from other GIA or geodynamic studies, however following

345 the method from van der Wal et al. (2015) allows to directly obtain absolute viscosity values from seismic measurements without the need to assume a background viscosity profile viscosity profile.

The results of the coupled model using a 3D rheology can be compared with the results using 1D rheologies. Two experiments are performed using a 1D rheology with two different upper mantle viscosity profiles: 10^{20} (hereafter referred to as 1D20) and

350   10^{21} Pa·s (hereafter referred to as 1D21). These values are consistent with the lower and upper boundaries of the upper mantle viscosity that is generally used in studies for Antarctica (e.g. Albrecht et al., 2020; Pollard et al., 2017; Gomez et al., 2018). The elastic lithospheric thickness is the same for both 1D experiments and is set to 100 km. Fig. S.4 in the supplementary materials shows the viscosity profile at 4 different locations for the 4 different rheologies. The locations are indicated by the numbers in Fig. 3a. At the Thwaites glacier (location I in Fig. 3a), the viscosity of the 3D rheologies is between 10^{20} and 10^{22}

355   Pa·s between 70 and 100 km depth, whereas the 1D rheologies assume this layer to be elastic. On the other hand, at dome C (location IV in Fig. 3a) the viscosity is above 10^{23} between 100 and 170 km depth for the 3D rheologies, whereas the 1D rheologies assume a viscosity of 10^{21} and 10^{20} Pa·s between 100 and 170 km depth. In general, the viscosity of the 3D rheologies are up to 4 orders of magnitude lower in West Antarctica and up to 3 orders of magnitude higher in East Antarctica compared to the 1D21 rheology. It should be noted that the response of the bedrock to changes in ice loading does not solely

360   depend on the local viscosity but on the viscosity of the whole region where the change in ice load occurs.
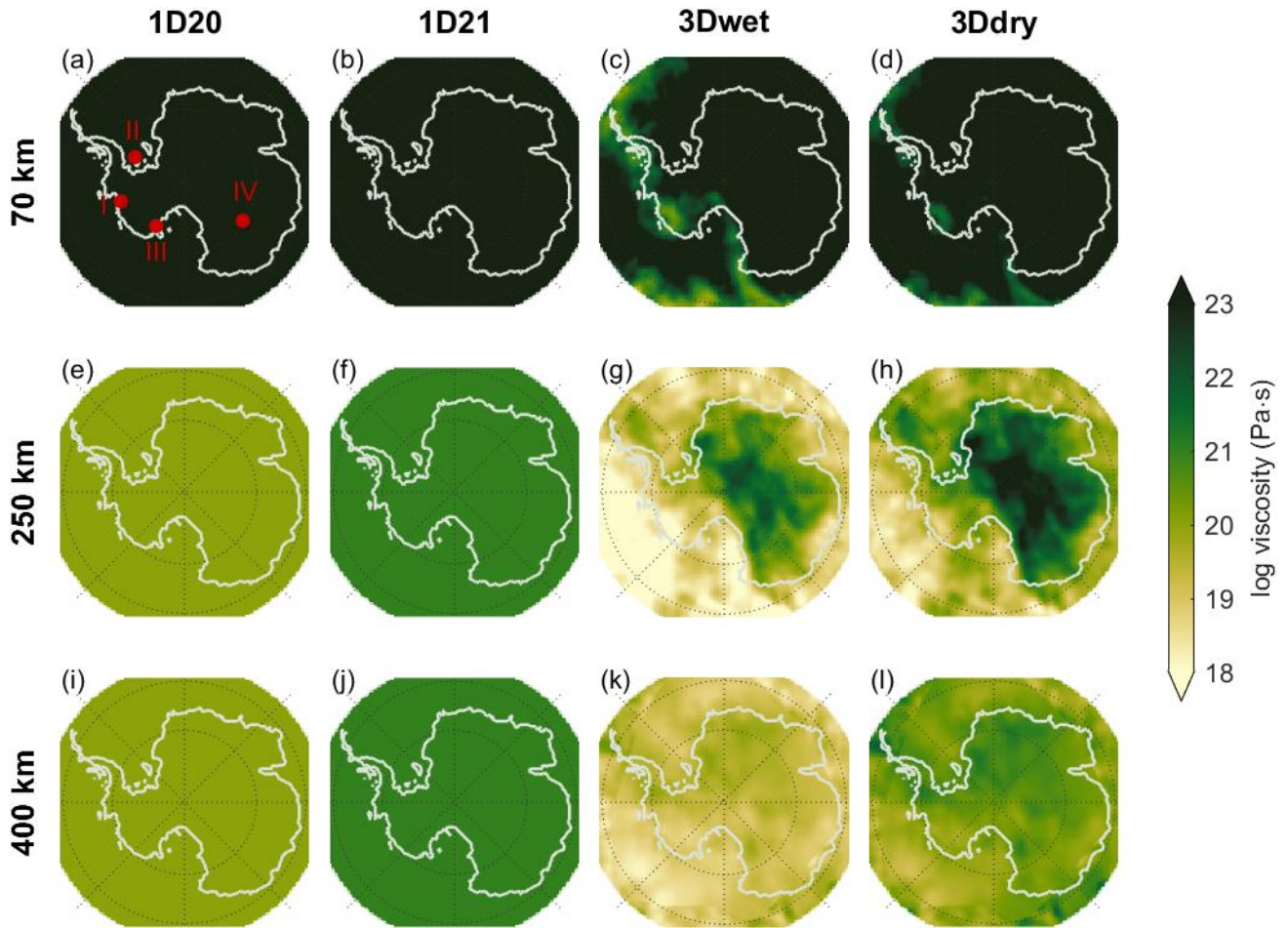
Figure 3: Panels a, e and i correspond to the 1D rheology referred to as 1D20. The red dots annotated by romain numbers in panel e correspond to the viscosity profiles shown in Fig. S.4 in the supplementary material. Panels b, f and j correspond to the 1D rheology referred to as 1D21. Panels a and b show a viscosity of 10^{44} Pa·s, representing the 100 km thick lithosphere in the 1D rheology. Panels c, g and k correspond to a 3D rheology with a water content of 500 ppm referred to as 3D (wet), and figures d, h and l correspond to a 3D rheology without water content referred to as 3D (dry). Both 3D rheologies assume a grain size of 4 mm. A pressure of 0.1 MPa is used to compute the viscosity from the dislocation and diffusion parameters.

2.3 Iterative coupling method

370 The simulation of ice dynamics for a certain coupling time step requires the deformation of the Earth over the coupling time step. On the other hand, the computation of the deformation over this coupling time step, using the GIA FE model, requires the change in ice mass over that coupling time step. For this study, an iterative coupling scheme has been developed that alternates between the models per time step with a varying length of 500 to 5000 yr. The GIA and ice-sheet model outputs (bedrock deformation and change in ice thickness respectively) are generated on different grids and the corresponding
375 interpolation method is described in the supplementary section. The iterative scheme is shown in Fig. 4. The ice thickness and deformation at each coupling time step of the coupled model is computed as follows:

1 Simulate the evolution of the AIS for the first coupling time step using ELRA. Use the difference in grounded ice thickness at the end of the coupling time step and the initial grounded ice thickness as input for the GIA FE model which starts initially in isostatic equilibrium.

2 Run the GIA FE model to compute the deformation of the Earth's surface during the first coupling time step. Next, subtract the final bedrock elevation of the coupling time step from the final bedrock elevation of the last time step and interpolate this linearly to obtain deformation at the time steps of the ice-sheet model. Run the ice-sheet model to compute the new ice sheet evolution at the first coupling time step using the updated deformation in linear increases during the coupling time step. The ice-sheet model and the GIA FE model uses its own internal time stepping, as discussed in section 2.1 and 2.2 respectively.

3 Continue the iterative process described in step 2 until a convergence criterium has been reached. The convergence of the coupled model and the required number of iterations is further described in section 2.3.2.

4 Take the average deformation of the last two iterations as the final deformation to minimize the uncertainties in areas where the coupled model does not converge to zero but alternates between positive and negative values. Pass the average deformation to the ice-sheet model and run the model to calculate the final ice sheet evolution over the first coupling time step.

5 All stresses present at the end of the first coupling time step are saved in the GIA FE model which will be restarted in the second coupling time step. The final configuration of the ice-sheet model at the end of the first coupling time step is also saved and used as starting point for the ice-sheet model simulation at the second coupling time step. The averaged deformation of the last two iterations of the previous coupling time step will be used as initial guess to run the ice-sheet model for the first iteration of the next coupling time step.

6 Once the simulation over the entire glacial cycle has finished, compute the difference between the simulated present day bedrock topography and the observed present day bedrock topography using eq. 6, as will be explained further in section 2.3.4. Then, repeat the simulation of the entire glacial cycle using a corrected initial topography. Repeat the glacial cycle 2 to 4 times to convergence to a simulated present day topography equal to the observed present day topography.
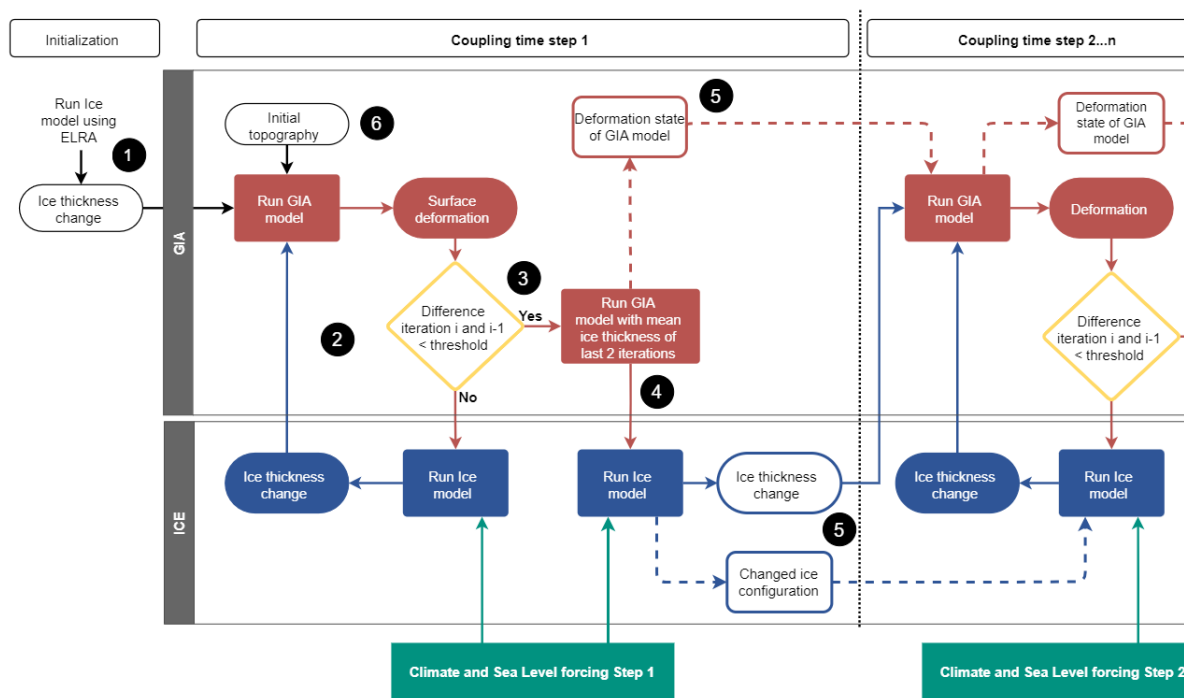
Figure 4: Schematic overview of the method for coupling the GIA and ice-sheet model. The numbers 1 to 6 in black circles refer to the steps of the iterative coupling process explained in the main text. The solid lines refer to the flow of input and output. The dashed lines connect the blocks for running the GIA or ice model to show that the saved model of the previous coupling time step is used to restart the model in the next coupling time step.

Gomez et al. (2018) create ice loading and bedrock deformation histories of 40 kyr with a temporal resolution of 200 yr and run the ice-sheet model and sea level model alternately at once over the full history. In the method of this study, the ice-sheet model and GIA FE model run alternately at each dynamic coupling time step, of which the coupling time step can be changed depending on the desired accuracy. However, the GIA FE model used in this study does not solve the sea level equation which should be included in the GIA FE model for realistic reconstructions. For this study, the last glacial cycle is simulated using 51 coupling time steps of 5000, 1000 and 500 yr (section 2.3.1). Tests are performed to determine the required number of iterations per coupling time step (section 2.3.3). After calculating the first glacial cycle there is usually a mismatch between modelled and observed topography at present-day. To solve this mismatch, we use two to four glacial cycle iterations, depending on the rheology, each with 51 coupling time steps to correct for the difference in modelled and observed topography (section 2.3.4) (e.g. Kendall et al., 2005). The method allows to use variable coupling time steps throughout the glacial cycle and between iterations of glacial cycles to decrease the total computation time.

2.3.1 Size of the coupling time step

A longer coupling time step increases the deformation and change in ice thickness over one coupling time step. Therefore, the coupling time steps need to be chosen sufficiently small, so that deformation and ice thickness change nearly linearly. On the other hand, a large coupling time step is desirable to limit the computation time. The convergence of the coupled model is highly dependent on the length of the coupling time step since the change in ice load, and thus the bedrock deformation, is smaller for smaller time steps, which converges faster.

The coupled model is tested using different coupling time steps for the 1D21 rheology. Relatively long coupling time steps of 5000 and 1000 yr are tested between 120 ka and 20 ka because the change in GIA signal is small within this period since the ice sheet volume is slowly increasing till LGM, and knowledge of the past climate is limited. Using a step size of 1000 yr did not lead to significantly different results than using time steps of 5000 yr and we therefore chose a step size of 5000 yr for the glaciation phase of the last glacial cycle. Because of the fast reduction of ice in a warming climate, smaller coupling time steps are required during the deglaciation. Han et al. (2022) showed that coupling time steps of 200 yr are optimal for the deglaciation phase in their coupled 1D GIA – ice-sheet model. However, their method assumes a constant topography during the coupling time step, which is not the case here, and the topography is updated only at the end of each time step. In our simulation, the topography changes linearly during the coupling time step and is updated every year in the ice-sheet model. In addition we run the ice-sheet model twice per coupling time step, whereas in the method of Han et al., (2022) this is done only once per coupling time step. The method of Han et al. (2022) therefore requires smaller coupling time steps between the GIA and ice-sheet models than the coupling method presented in this study. To determine the length of the coupling time step of the deglaciation phase, we tested a step size of 200 and 500 yr over the period of fast deglaciation between 15 and 5 ka. The results are shown in Fig. S.5 in the supplementary materials, together with a table showing the exact used step sizes over the glacial cycle (Table S.1). Difference in bedrock elevation between using a step size of 200 and 500 yr occurs mainly at the Ross embayment and the Princess Astrid Coast of Queen Maud land and bedrock is maximum 20 meter higher at present day when a time step of 200 yr is used. The ice thickness of the Ross Ice Shelf at present day is 70 meter larger when a step size of 200 yr is used and there is no difference in grounding line position. The ice thickness at the Princess Astrid Coast at present day is 680 meter larger and the grounding line lies 80 meter further inland when a step size of 200 yr is used. However, this region with large ice thickness differences is very small and spans only 120 km. The computation time of simulating a time step of 200 yr and 500 yr is similar but the 200 yr time step requires 42 extra time steps. Using time steps of 200 yr between 15 and 5 ka increases the computation time with 56 hours. We therefore chose to use time steps of 500 yr during the deglaciation phase. We used time steps of 1000 yr around LGM and between 5 and 1 ka to create a smooth transition between the glaciation phase, the deglacation phase and the Late Holocene. The chosen time steps for the entire glacial cycle for this study are shown in Table 2.

Table 2: Coupling time steps over last glacial cycle.

Period [ka]	Time step size [kyr]	Number of coupling times
120 – 20	5	20
20 – 15	1	5
15 – 5	0.5	20
5 – 1	1	4
1 - 0	0.5	2

2.3.2 Convergence of the coupled model

The number of iterations needed to converge is dependent on the change in ice load and the Earth's structure. The coupled model requires 3 to 13 iterations iterations per coupling time step to converge to an incremental change in deformation of less than 3 mm per yr in all individual grid cells when using the 1D21 rheology. A different rheology requires a different number of iterations. An example of convergence of a coupling time step using the 1D21 rheology can be seen in Fig. 5, which shows the difference in deformation and ice thickness between iterations of one coupling time step from 120 ka till 115 ka. The deformation threshold is set to 15 m for the entire glacial cycle. Panel a of Fig. 5 shows the change in ice thickness and panel b shows the change in bedrock elevation over this coupling time step when using the 1D21 rheology. Panels c to f show the difference in ice thickness and bedrock elevation compared to the former iteration. The ice thickness and deformation converge for most of Antarctica, except at the Ross embayment where the shelf thickness still differs between iteration 2 and 3 due to its high sensitivity to grounding line position.

When using the 1D20 rheology, ice thickness and deformation do not converge exactly at multiple locations around the grounding line after iteration 3. A high deformation rate and large changes in ice thickness cause a large shift in the position of the grounding line. Glaciated grid cells of the ice-sheet model are defined as grounded ice or floating ice, depending on their position upstream or downstream of the grounding line. If the grounding line in the ice-sheet model moves with every iteration due to large changes in deformation, the grid cells around the grounding line alternate between an ice shelf and grounded ice status. Since ice thickness can differ with hundreds of meters between adjacent grid cells, the difference in ice thickness at one grid cell between iterations can also differ greatly. In this case, both ice thickness and the change in deformation at these grid cells around the grounding line do not converge to zero but to an alternating value. The bedrock deformation converges better than ice thickness because of the stiffness of the Earth causing a more smooth deformation pattern.

Figure 5: Iterations of coupling time step 1 from 120 ka to 115 ka using the 1D21 rheology. (a) Change in ice thickness over this coupling time step. (b) Change in bedrock elevation over this coupling time step. (c-f) Difference in ice thickness and bedrock elevation change compared to the previous iteration. The threshold is set to 10 m over the full coupling time step.

Tests show that the coupled model converges within an acceptable computation time when the convergence criterium is set to 3 mm per yr over the coupling time step. This uncertainty is still below the effect of the uncertainties of the input parameters such as background mantle temperature and seismic velocity (e.g. Blank et al. 2021) . Since the grid cells around the grounding line in some cases do not converge to zero, the coupling method introduces an uncertainty. For example, if in one grid cell the change in total deformation over 5000 yr keeps alternating between -2 and +2 meter, the uncertainty range is 4 meter. To decrease this uncertainty, the average deformation of the last two iterations is used as the final deformation to simulate ANICE for the final iteration of the time step. Decreasing the spatial resolution would allow smoother transitions between grounded and floating ice and thus a further improvement of the convergence. However, the ice-sheet model is currently limited to a 40 kilometer resolution.

2.4.3 Number of iterations per coupling time step

Three simulations are conducted to study the effect of the number of iterations on the GIA and the evolution of the AIS using the 1D21 rheology. One simulation is performed with 1 iteration per time step (which means that the ice-sheet model is ran twice over the coupling time step and the GIA FE model is ran one time over the coupling time step), one simulation with a varying number of iterations per time step using the convergence threshold as described in section 2.3.2 and one simulation simulates first the full glacial cycle using the ice-sheet model, followed by a full glacial cycle using the GIA FE model, and last another glacial cycle using the ice-sheet model. Differences in deformation and ice thickness between the three simulations are neglectable during the glaciation phase of the last glacial cycle. At present day, the absolute maximum difference between the convergence simulation and the simulation with only 1 iteration is 700 m in ice thickness at the Ross embayment and the grounding line differs by 80 km in this region (Fig. S.6 in the supplementary materials). The maximum difference in ice thickness at present-day is still 2 times smaller than the maximum difference between using different 1D and 3D rheology's and only occurs over very small regions. The absolute maximum difference between the 1 iteration simulation and simulation where the entire cycle is ran at once is much larger with 3500 m in ice thickness at the Ross embayment, and the grounding line differs by approximately 800 km in this region (Fig. S.7 in the supplementary materials). From this we conclude that the effect of iterating over the glacial cycle versus iterating per coupling time step is much larger than the effect of the number of iterations over a coupling time step. Furthermore, the effect of decreasing the length of the coupling time step is small.

Reducing the number of iterations significantly reduces the computation time. The coupled model simulations are performed on 16 CPU's of model Intel(R) Xeon(R) Gold 6140 CPU @ 2.30GHz, of which the CPU speed varies between 1085 and 2707 MHz. The GIA FE model takes approximately 20 and 40 minutes to simulate 5000 yr for the 1D rheology and the 3D rheology respectively. The ice-sheet model takes only several minutes so the GIA FE model takes most of the time. A simulation of one glacial cycle using the 1D GIA FE model performing 3 iterations per coupling time step takes 27 days when running on 16 CPU's performing 51 time steps (which is 1 glacial cycle). Performing only one iteration reduces the total running time to 30 hours. Simulating the last glacial cycle using a 3D GIA FE model takes about 5 days when only 1 iteration per time step is performed, and 37 days when in total 293 iterations are performed.

Considering the long computation time if multiple iterations are used, only 1 iteration is used for results in the remainder of the paper. This means that for each coupling time step first the ice model is run using the deformation over the former coupling time step, next the GIA FE model is run with the new ice load from the ice model and finally, the ice model is run including the new deformation of the GIA FE model.

2.3.4 Iterations over the entire glacial cycle

The bedrock elevation at last glacial maximum is higher for a larger mantle viscosity since there is less subsidence during the glaciation phase. In that case, the ice sheet in West Antarctica will melt less and less bedrock uplift will occur during the deglaciation phase. Thus, the differences in melt during the deglaciation phase for the various rheologies could be caused not
525 only by the direct effect of the viscosity of the rheology on the uplift, but by the difference in bedrock elevation at last glacial maximum. The direct effect of various rheologies on ice dynamics during the deglaciation phase can be isolated if the model is constrained by ending up at present with the observed bedrock topography. Without iterations, the present-day bedrock topography after a glacial cycle differs per simulation and does not equal the observed bedrock topography. For this reason we apply a commonly used approach in GIA modelling by applying several iterations of the entire last glacial cycle, hereafter
530 called glacial iterations, as described in step 6 of the coupling scheme in Fig. 4. They are needed to ensure that modelled and observed present day bedrock topography are in agreement (Peltier, 1994; Kendall et al., 2005). It is assumed here that this difference is solely caused by modelled vertical GIA deformation, neglecting other types of deformation, such as tectonic motion and erosion or shortcomings in the ice-sheet model.

535 The initial bedrock topography at 120 ka of the first glacial iteration is initially assumed to be equal to present-day bedrock topography, taken from ALBMAP (Le Brocq et al., 2010). For the next glacial iterations, the initial bedrock topography is adjusted for the difference in simulated present-day bedrock topography and the observed present-day topography ALBMAP:

$$b_{0,i} = b_{0,i-1} + (b_{ALBMAP)} - b_{PD,i-1}) , \tag{6}$$

Where the subscript i refers to the iteration over the glacial cycle, $b_{0,i}$ refers to the bedrock elevation at the beginning of the
540 new glacial iteration, $b_{0,i-1}$ refers to the bedrock elevation at the beginning of the previous glacial iteration, $b_{PD,i-1}$ refers to the present-day bedrock elevation of the last glacial iteration and $b_{ALBMAP)}$ refers to the observed present-day bedrock topography based on Le Brocq et al. (2010). Four to five iterations of the entire glacial cycle are typically needed to converge the modelled present-day bedrock topography to the observed present-day bedrock topography, of which the first three iterations are shown in Fig. S.8 in the supplementary materials.

545 ### 3 Results and discussion

3.1 Testing the coupled model using different 1D rheologies

The evolution of the AIS over the entire last glacial cycle shows a similar ice sheet thickness, extent and volume using the 1D coupled model of this study, compared to other studies using coupled 1D GIA – ice-sheet models and coupled ELRA – ice-sheet models (de Boer et al., 2014, 2017; Gomez et al., 2015; Pollard et al., 2017). To further test if the coupled model works
550 as expected, the results for an upper mantle viscosity of 10^{20} Pa·s (1D20) are compared to those of 10^{21} Pa·s (1D21). The

results of both simulations in terms of ice thickness and grounding line position follow a similar pattern as in Pollard et al. (2017). The Filchner-Ronne and Ross embayment (indicated with FR and R respectively in Fig. 6a) remain larger during the deglaciation phase for the 1D20 simulation than for the 1D21 simulation because the uplift is faster when using the smaller mantle viscosity of 10^{20} Pa·s (Fig. 6). Based on the Marine Ice Sheet Instability (MISI) process, increased ice shelf melt and

555   fast grounding line retreat can be expected due to a retrograde bedrock slope and an increasing relative sea level caused by subsidence (Schoof, 2007). At present day, the ice is up to 1 km thinner around the grounding line of the Ross and Filchner-Ronne embayments, and the grounding line is further retreated by approximately 100 km at the Ross embayment in the 1D21 results compared to the 1D20 results, shown in Fig. 6h.
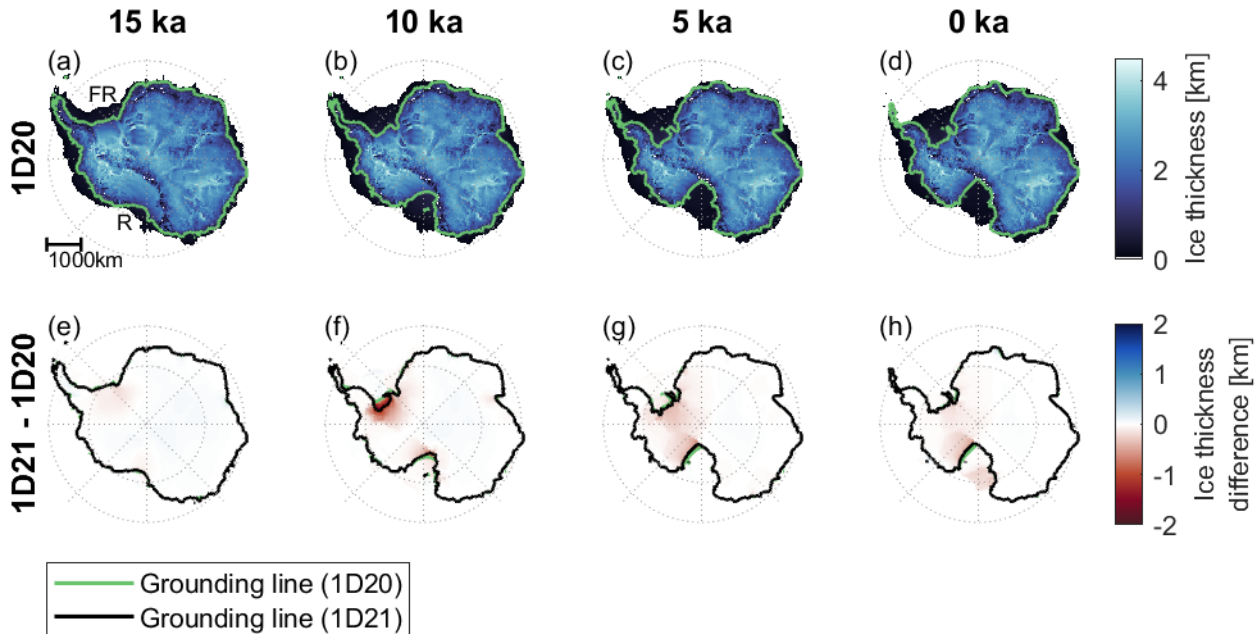
Figure 6: Ice thickness of 1D20 (top row) and the difference in ice thickness between 1D20 and 1D21 (bottom row) at four epochs during the deglaciation phase. (a) FR refers to the Filchner-Ronne Ice Shelf and R refers to the Ross embayment. **In (e-h), the 1D20 grounding line (green) mostly overlaps with the 1D21 grounding line (black).**

3.2 Stabilization of the AIS using 1D and 3D rheologies.

565   In a cooling climate between 120 ka and 20 ka, all 1D and 3D coupled simulations show an ice thickness increase mainly at the Ross and the Filchner-Ronne embayments and at the Peninsula, causing the bedrock to subside in these regions. In the 1D simulations, the bedrock subsides 500 m less during this period than in the 3Ddry simulations due to the stiffer 1D rheology compared to the 3Ddry rheology (Fig. 7a and 7d). However, the bedrock subsides a similar amount when using the 3Dwet rheology compared to the 1D20 rheology during the glaciation phase. At the Amundsen embayment, the mantle viscosity of

570   the 3Dwet rheology is so low that the bedrock responds quickly to slight changes in ice loading. The ice loading follows a

fluctuating pattern due to the atmospheric and sea level forcing (Fig. S.1 in the supplementary materials) and the bedrock follows the same pattern, although dampened and delayed. The bedrock with the 3Dwet rheology subsides over the full glaciation phase but not as much as the bedrock with the 3Ddry rheology because the 3Dwet rheology can respond fast enough to cause uplift in periods when ice thickness does not grow as much.

575

At LGM, the ice thickness is several hundreds of meter larger near the Ross and the Filchner-Ronne embayments when using a 1D rheology compared to the 3Ddry rheology (Fig. 8bc). During the deglaciation phase, the Ross and Filchner-Ronne embayments retreat fast due climate warming, similar to what other studies of the AIS evolution suggest (e.g. Albrecht et al., 2020). The 1D mantle viscosity leads to a slower uplift which causes the grouding line near the Ross and Filchner-Ronne embayments to retreat faster in the 1D simulations than in the 3D simulation (Fig. 7b-c, e-f), corresponding to results by Pollard et al. (2017) and Gomez et al. (2018). Using a 3Ddry rheology leads to a difference in grounding line position of up to 700 km and a difference in ice thickness of up to 2 km at present-day along the Siple coast (Fig. 8c). Using a 3Dwet rheology leads to 600 m thicker ice at present day compared to using the 1D20 rheology and a more advanced grounding line position of 80 km. The ice thickness of the 3Dwet rheology lies closer to the 1D20 ice thickness than the ice thickness of the 3Ddry rheology because the bedrock elevation at LGM is similar for the 1D20 and the 3Dwet rheologies and is 500 m lower for the 3Ddry rheology. Due to the lower bedrock elevation at LGM when the 3Ddry rheology is used, the ice sheet in West Antarctica will melt more and faster bedrock uplift will occur during the deglaciation phase when a stronger rheology is used. The differences in melt during the deglaciation phase between using different rheologies is then not caused by the direct effect of different rheologies on uplift rates, but by the difference in bedrock elevation at last glacial maximum.

590

In contrast to the changes in West Antarctica, Fig. 8 shows that the difference in ice sheet thickness between the 1D and 3Ddry simulations in the interior of the East AIS are not larger than 50 meter, although the mantle viscosity in East Antarctica is several orders of magnitude higher in the 3D rheology than in the 1D rheologies. This is because the interior of the ice sheet is not as sensitive to the bedrock elevation as the outlet glaciers near the margin, leading to an insignificant effect of mantle viscosity differences. The interior of Antarctica is also less sensitive to changes in the surface temperature and sea level and therefore follows an equilibrium response which is independent of the rheology.
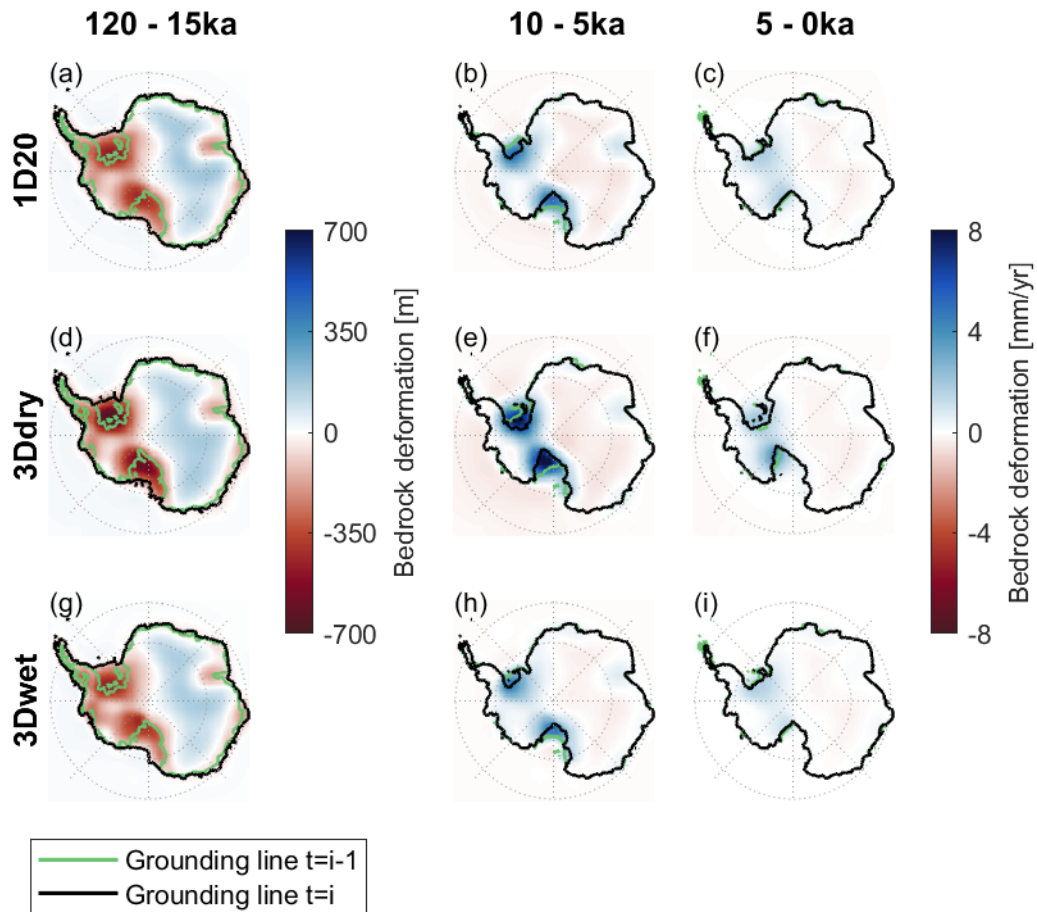
Figure 7: Uplift over the glaciation phase (120-15ka) for 1D20 (panel a), 3Ddry (panel d) and 3Dwet (panel g), and average uplift rates between 10ka and present day for the 1D20 (panels b,-c), 3Ddry (panels e,f) and 3Dwet (panels h,i) rheologies. The green grounding line shows the grounding line position at the beginning of the period over which the uplift or uplift rate is computed, and the black grounding line shows the position at the end of the period.
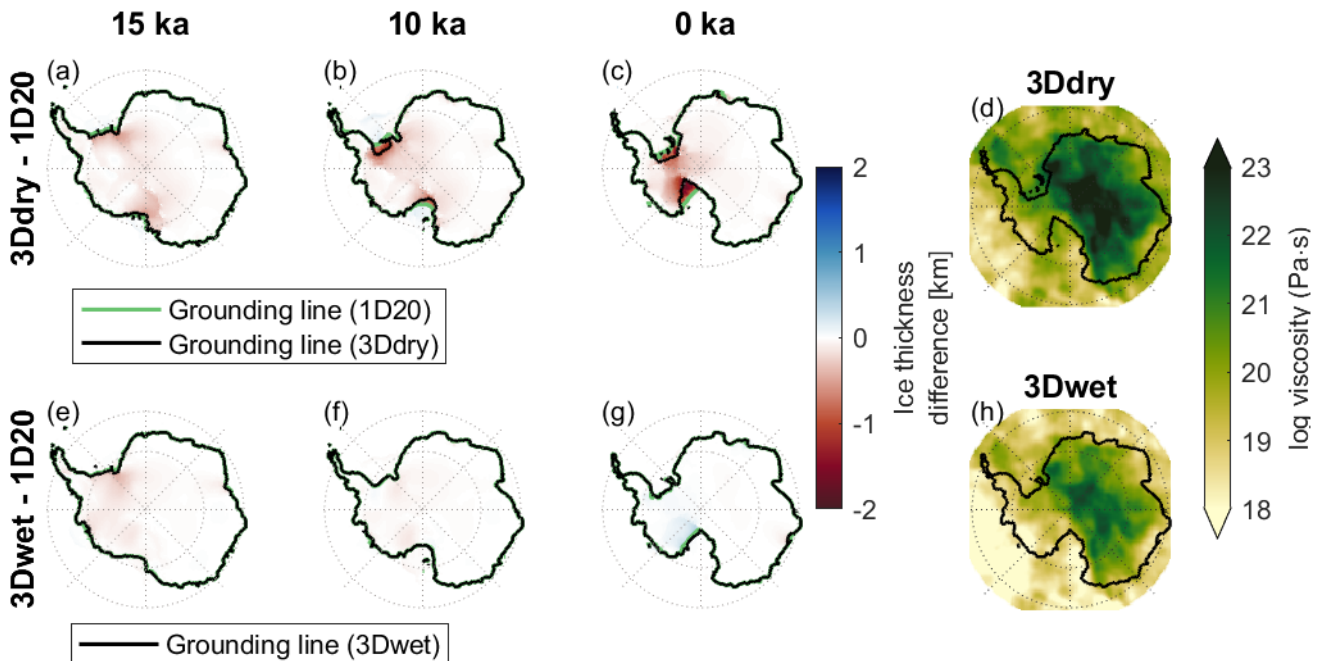
Figure 8: 1D vs 3D ice thickness and mantle viscosity at a depth of 250 km. A stress of 0.1 MPa is used to compute the 3D viscosity from dislocation and diffusion parameters. In Fig 8, the 1D grounding line (green) mostly overlaps with the 3D grounding lines (black).

As can be seen in Fig. 8, Antarctic ice mass variability is dominated by the changes in West Antarctica. Figure 9 shows that 1D21 decreases faster than the 1D20 rheology dues to the slower uplift in West Antarctica as shown in Figure S.9 in the supplementary materials. Figure 9 also shows that the present-day ice volume is 0.2-0.6 km^3 lower when using 1D rheologies compared to using the 3Dwet rheology. The use of the 3Dwet rheology stabilizes the ice sheet compared to the use of a 1D mantle viscosity (Fig. 9) because a lower mantle viscosity at West Antarctica stabilizes the Filchner-Ronne and Ross embayments (Fig. 8). However, the ice volume decreases faster in the deglaciation phase for the 3Ddry rheology compared to the 1D rheologies. That is because the ice volume and ice surface elevation when using the 3Ddry rheology is much lower at LGM than the ice volume when one of the other rheologies is used and the bedrock uplift during the deglaciation phase is not fast enough to prevent the ice sheet from melting more ice compared to the using the other rheologies. The bedrock elevation at LGM plays therefore a very important role to determine the ice sheet evolution during the deglaciation phase.

Gomez et al. (2018) found an insignificant difference in ice volume at present-day for 3D viscosity vs 1D viscosity. Gomez et al. (2018) included the effect of regional sea level in the coupled model. Including this effect in our model would decrease ice shelf melt and therefore decrease the ice volume change itself and the difference in ice volume between the 1D and 3D simulations. Differences in terms of ice dynamics formulations, forcings, rheology and resolution could additionally explain the different result of Gomez et al. (2018) and this study.
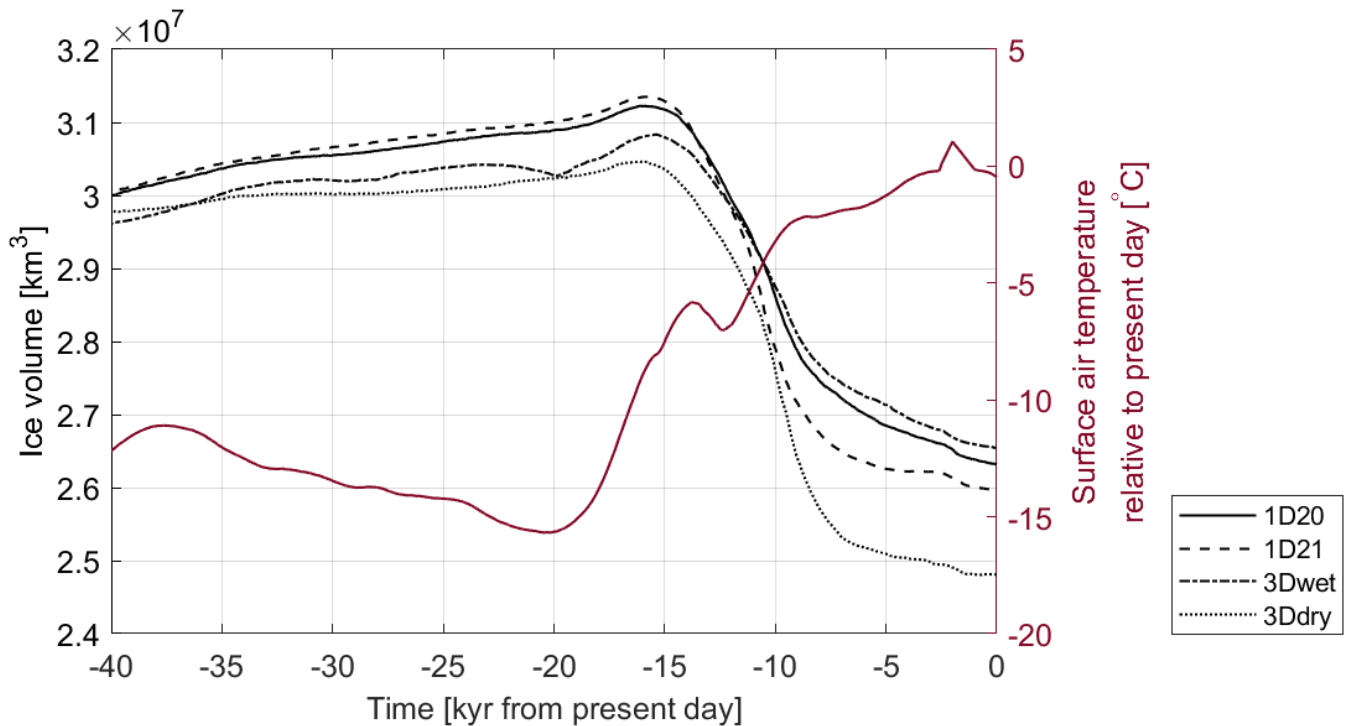
625 **Figure 9: The black lines show the AIS volume over time for the 1D simulations and for the two 3D simulations (dry and wet rheology). The red line shows the mean surface temperature.**

Overall, it can be concluded that the variations in mantle viscosity between a realistic 3D rheology and commonly used 1D rheology have a significant impact on grounding line position and ice thickness in West Antarctica and an insignificant impact in East Antarctica. Furthermore, during the deglaciation phase the difference in ice thickness of the 3Dwet and the 1D20 simulations is smaller than the difference of the 3Ddry and the 1D20 simulations because the bedrock elevation at LGM is much lower when the 3Ddry is used. The ice thickness is lower for the Ross and Filchner-Ronne embayments when using a 1D rheology compared to the 3Dwet rheology, but much higher compared to the 3Ddry rheology. The stabilizing effect increases when using the 3Dwet rheology compared to using the 1D rheologies because the mantle viscosity under West Antarctica is lower and shows fast uplift during the deglaciation phase. Ice-sheet models using a similar 1D rheology with an upper mantle viscosity of 10^{20} Pa·s or higher and a lithospheric thickness of 100 km (e.g. DeConto et al., 2021; Pollard et al., 2017; Konrad et al., 2015), might therefore underestimate the stability for the Ross and Filchner-Ronne embayments.

4   Conclusions and outlook

This study presented the first method to study GIA feedback on ice dynamics for laterally varying mantle viscosity on short timescales of hundreds of years using a coupled ice sheet-3D GIA FE model. Each coupling time steps needs iterations to include the GIA feedback on short timescales of 500 to 5000 yr. The coupling method is tested for convergence, which is

mainly dependent on the size of the time step. We used only one iteration per time step with a variable coupling time step of 500 to 5000 yr. Two to four iterations over the entire cycle are needed to adjust the initial topography to arrive at the present-day topography at the end of the simulation. Experiments where the resolution in near field and far field are varied indicate that a near field resolution of 30 by 30 km and a far field of 200 by 200 km yields an accuracy of 2 mm/yr bedrock deformation and a computation time of 5 days to simulate a single glacial cycle.

We created two 3D Earth rheologies based on an Antarctic-wide seismic model. Using the 3Ddry Earth rheology leads to a difference in grounding line position up to 700 km and a difference in ice thickness of up to 3500 m compared to using a 1D mantle viscosity of 10^{20} Pa·s at present, due to a much lower bedrock elevation at LGM (Fig. 8). The bedrock elevation at LGM is similar between using the 3Dwet Earth rheology and a 1D mantle viscosity of 10^{20} Pa·s because the mantle viscosity at the Amundsen embayment is so low that uplift can occur during short periods of atmospheric temperature decrease in the glaciation phase. Using the 3Dwet Earth rheology leads to a less retreated grounding line position of up to 80 km and thicker ice thickness of up to 600 m compared to using a 1D mantle viscosity of 10^{20} Pa·s at present day (Fig. 8). The ice volume at present day increases with 0.5 or 1.8 percent when using the 3Dwet rheology compared to using a 1D mantle viscosity of 10^{20} Pa·s or 10^{21} Pa·s respectively. That is because the low mantle viscosity found in the 3Dwet rheology leads to large uplift rates which stabilize the ice sheet more than the 1D rheologies. An ice-sheet model coupled to a 1D rheology with an upper mantle viscosity of 10^{20} Pa·s or 10^{21} Pa·s and lithospheric thickness of 100 m underestimates the stabilizing effect of GIA. However, when the bedrock elevation at LGM is much lower, such as for the 3Ddry rheology compared to the 1D rheologies, the difference in ice volume is up to 0.2 km^3 between the 3Ddry and the 1D rheologies. In the future it is desired to apply the coupling method presented in this paper with high resolution models including regional sea level forcing, not only because a higher resolution provides more accurate grounding line simulation, but also because the method will converge better since the grid cell is smaller and thus the ice load on one grid cell as well.

The method developed for this study has several advantages which can be exploited in future work when simulation are performed which are as realistic as possible, rather than focussing on the physical principles as we did in this paper. First, the time step is variable throughout the glacial cycle and can be adjusted between iterations of the full glacial cycles. This way, computation time can be saved by simulating the first glacial cycle on a low temporal resolution to obtain the first modelled present-day topography, while the second iteration with the adjusted initial topography can be performed with a higher temporal resolution to include the GIA feedback more accurately. Second, the GIA FE model can be restarted at any time step. Therefore, the last glacial cycle can once be simulated on a very high temporal resolution to obtain present-day results and the coupled model can be restarted from present-day to simulate future evolution of the ice sheet under different scenarios or rheologies. Third, the coupling method allows coupling with any ice-sheet model, as long as the model can restart at each coupling time step. Last, the method has potential for a higher temporal resolution than used in this study at designated periods

in time. For example, the simulation can be restarted at 500 yr before present and run on a higher temporal resolution such as a coupling time step of 10 yr to simulate recent uplift and future climate change projections.

Code and data availability

"The model, the data, and the MATLAB scripts to generate the figures included in this manuscript are freely available via the doi 10.4121/19765816.v2 for the model, and the doi 10.4121/19772815.v2 for the data. The model and data are accessible via the following websites respectively: https://doi.org/10.4121/19765816.v2 and https://doi.org/10.4121/19772815.v2.

Author contribution

CC and WW designed the method. BdB, BB and CC developed the models used. CC performed the simulations. WW and RW contributed to debugging and the interpretation of the results. CC prepared the manuscript with contributions from all co-authors.

Competing interests

The authors declare that they have no conflict of interest.

Acknowledgements

This project has received funding from the European Union's Horizon 2020 research and innovation programme under grant agreement No 869 304, PROTECT contribution number 28, and from the 3D Earth project funded by ESA as Support to Science Element. We want to thank Maryam Yousefi, Pippa Whitehouse and Volker Klemann for their constructive feedback on the manuscript. This lead to a significantly improved model and manuscript.

References

A,G., Wahr, J., and Zhong, S.: Computations of the viscoelastic response of a 3-D compressible Earth to surface loading: an application to Glacial Isostatic Adjustment in Antarctica and Canada. Geophysical Journal International, 192, 557-572, doi:10.1093/gji/ggs030, 2013.

Adhikari, S., Ivins, E.R., Larour, E., Seroussi., H., Morlighem., M., and Nowicki., S.: Future Antarctic bed topography and its implications for ice sheet dynamics. Solid Earth, 5, 569-584, doi:10.5194/se-5-569-2014, 2014.

Albrecht, T., Winkelmann, R., and Levermann, A.: Glacial-cycle simulations of the Antarctic Ice Sheet with the Parallel Ice Sheet Model (PISM) – Part 1: Boundary conditions and climatic forcing. The Cryosphere, 14, 633-656, doi:10.5194/tc-14-599-2020, 2020.

Barletta, V.R., Bevis, M., Smith, B.E., ..., and Smalley, R.: Observed rapid bedrock uplift in Amundsen Sea Embayment promotes ice-sheet stability. Science, 360, 1335-1339, doi:10.1126/science.aao1447, 2018.

Becker, T.W., and Boschi, L.: A comparison of tomographic and geodynamic mantle models. Geochemistry, Geophysics, Geosystems, 3, doi:10.1029/2001GC000168, 2002.

Berends, C.J., de Boer, B., and van de Wal, R.S.W.: Application of HadCM3@ Bristolv1. 0 simulations of paleoclimate as forcing for an ice-sheet model, ANICE2. 1: set-up and benchmark experiments. Geoscientific Model Development, 11, 4657-4675, doi:10.5194/gmd-11-4657-2018, 2018.

Berends, C.J., De Boer, B., Dolan, A.M., Hill, D.J., and Van De Wal, R.S.W.: Modelling ice sheet evolution and atmospheric CO_2 during the Late Pliocene. Climate of the Past, 15, 1603-1619, doi:10.5194/cp-15-1603-2019, 2019.

Bintanja, R., van de Wal, R., and Oerlemans, J.: Modelled atmospheric temperatures and global sea levels over the past million years. Nature, 437, 125–128, doi:10.1038/nature03975, 2005.

Bintanja, R., and van de Wal, R.: North American ice-sheet dynamics and the onset of 100,000-year glacial cycles. Nature, 454, 869–872, doi:10.1038/nature07158, 2008.

Blank, B., Barletta, V., Hu, H., Pappa, F., and van der Wal, W.: Effect of Lateral and Stress-Dependent Viscosity Variations on GIA Induced Uplift Rates in the Amundsen Sea Embayment. Geochemistry, Geophysics, Geosystems, 22, e2021GC009807, doi:10.1029/2021GC009807, 2021.

Bradley, S.L., Reerink, T.J., van de Wal, R.S.W., and Helsen, M.M.: Simulation of the Greenland Ice Sheet over two glacial–interglacial cycles: investigating a sub-ice- shelf melt parameterization and relative sea level forcing in an ice-sheet–ice-shelf model. Climate of the Past, 14, 619–635, doi:10.5194/cp-14-619-2018, 2018.

Bueler, E., Lingle, C.S., and Brown, J.: Fast computation of a viscoelastic deformable Earth model for ice-sheet simulations. Ann. Glaciol., 46, 97–105, doi:10.3189/172756407782871567, 2007.

Bueler, E., and Brown, J.: Shallow shelf approximation as a "sliding law" in a thermomechanically coupled ice sheet model. Journal of Geophysical Research: Earth Surface, 114, F03008, doi:10.1029/2008JF001179, 2009.

Coulon, V., Bulthuis, K., Whitehouse, P. L., Sun, S., Haubner, K., Zipf, L., & Pattyn, F.: Contrasting response of West and East Antarctic ice sheets to glacial isostatic adjustment. Journal of Geophysical Research: Earth Surface, 126, doi:10.1029/2020JF006003, 2021.

De Boer, B., Van De Wal, R.S.W., Lourens, L.J., Bintanja, R., and Reerink, T.J.: A continuous simulation of global ice volume over the past 1 million years with 3-D ice-sheet models. Climate Dynamics, 41, 1365–1384, doi:10.1007/s00382-012-1562-2, 2013.

De Boer, B., Stocchi, P., and Van De Wal, R.S.W.: A fully coupled 3-D ice-sheet-sea-level model: algorithm and applications. Geoscientific Model Development, 7, 2141-2156, doi:10.5194/gmd-7-2141-2014, 2014.

De Boer, B., Stocchi, P., Whitehouse, P.L., and Van De Wal, R.S.W.: Current state and future perspectives on coupled ice-sheet–sea-level modelling. Quaternary Science Reviews, 169, 13-28, doi:10.1016/j.quascirev.2017.05.013, 2017.

DeConto, R.M., Pollard, D., Alley, R.B., Velicogna, I., Gasson, E., Gomez, N., ... and Dutton, A.: The Paris Climate Agreement and future sea-level rise from Antarctica. Nature, 593, 83-89, doi:10.1038/s41586-021-03427-0, 2021.

Fullea, J., Lebedev, S., Martinec, Z., and Celli, N.L.: WINTERC-G: mapping the upper mantle thermochemical heterogeneity from coupled geophysical–petrological inversion of seismic waveforms, heat flow, surface elevation and gravity satellite data. Geophysical Journal International, 226, 146-191, doi:10.1093/gji/ggab094, 2021.

Geruo, A., Wahr, J., Zhong, S.: Computations of the viscoelastic response of a 3-D compressible Earth to surface loading: an application to Glacial Isostatic Adjustment in Antarctica and Canada. Geophysical Journal International, 192, 557–572, doi:10.1093/gji/ggs030, 2013.

Goes, S., Govers, R., and Vacher, A.P.: Shallow mantle temperatures under Europe from P and S wave tomography. Journal of Geophysical Research: Solid Earth, 105, 11153-11169, doi:10.1029/1999JB900300, 2000.

Gomez, N., Mitrovica, J.X., Tamisiea, M.E., and Clark, P.U.: A new projection of sea level change in response to collapse of marine sectors of the Antarctic Ice Sheet. Geophysical Journal International, 180, 623-634, doi:10.1111/j.1365-246X.2009.04419.x, 2010.

Gomez, N., Pollard, D., Mitrovica, J.X., Huybers, P., and Clark, P.U.: Evolution of a coupled marine ice sheet–sea level model. Journal of Geophysical Research: Earth Surface, 117, doi:10.1038/NGEO1012, 2012.

Gomez, N., Pollard, D., and Mitrovica, J.X.: A 3-D coupled ice sheet – sea level model applied to Antarctica through the last 40 ky. Earth and Planetary Science Letters, 384, 88-99, doi:10.1016/j.epsl.2013.09.042, 2013.

Gomez, N., Pollard, D. and Holland, D.: Sea-level feedback lowers projections of future Antarctic Ice-Sheet mass loss. Nature Communications, 6, 8798, doi:10.1038/ncomms9798, 2015.

Gomez, N., Latychev, K., and Pollard, D.: A Coupled Ice Sheet–Sea Level Model Incorporating 3D Earth Structure: Variations in Antarctica during the Last Deglacial Retreat. Journal of Climate, 31, 4041–4054, doi:10.1175/JCLI-D-17-0352.1, 2018.

Gomez, N., Weber, M. E., Clark, P. U., Mitrovica, J. X., & Han, H. K.: Antarctic ice dynamics amplified by Northern Hemisphere sea-level forcing. Nature, 587, 600-604, doi:10.1038/s41586-020-2916-2, 2020.

Gordon, R.B.: Diffusion creep in the Earth's mantle. Journal of Geophysical Research, 70, 2413-2418, doi:10.1029/JZ070i010p02413, 1965.

Han, H.K., Gomez, N., and Wan, J.X.W.: Capturing the interactions between ice sheets, sea level and the solid Earth on a range of timescales: a new "time window" algorithm. Geoscientific Model Development, 15, 1355-1373, doi:10.5194/gmd-15-1355-2022, 2022.

Hay, C.C., Lau, H.C., Gomez, N., ... and Wiens, D.A.: Sea level fingerprints in a region of complex Earth structure: The case of WAIS. Journal of Climate, 30, 1881-1892, doi:10.1175/JCLI-D-16-0388.1, 2017.

Heeszel, D.S., Wiens, D.A., Anandakrishnan, S., ... and Winberry, J.P.: Upper mantle structure of central and West Antarctica from array analysis of Rayleigh wave phase velocities. Journal of Geophysical Research: Solid Earth, 121, 1758-1775, doi:10.1002/2015JB012616, 2016.

Hibbitt, D., Karlsson, B. and Sorensen, P.: Getting Started with ABAQUS, Version (6.14), Hibbitt, Karlsson & Sorensen, Inc, 2016.

Hirth, G., and Kohlstedt, D.: Rheology of the upper mantle and the mantle wedge: A view from the experimentalists. Geophysical Monograph-American Geophysical Union, 138, 83-106, doi:10.1029/138GM06, 2003.

Hu, H., van der Wal, W., and Vermeersen, L.L.A.: A numerical method for reorientation of rotating tidally deformed viscoelastic bodies. Journal of Geophysical Research: Planets, 122, 228-248, doi:10.1002/2016JE005114, 2017.

Ivins, E.R., van der Wal, W., Wiens, D.A., Lloyd, A.J., and Caron, L.: Antarctic upper mantle rheology. Geological Society, London, Memoirs, 56, doi:10.1144/M56-2020-19, 2021.

Karato, S.I., Paterson, M.S., and FitzGerald, J.D.: Rheology of synthetic olivine aggregates: influence of grain size and water. Journal of Geophysical Research: Solid Earth, 91, 8151-8176, doi:10.1029/JB091iB08p08151, 1986.

Karato, S.I., Jung, H., Katayama, I., and Skemer, P.: Geodynamic signific.ance of seismic anisotropy of the upper mantle: new insights from laboratory studies. Annual Review of Earth and Planetary Sciences, 36, 59-95, doi:10.1146/annurev.Earth.36.031207.124120, 2008.

Kaufmann, G., Wu, P., and Ivins, E.R.: Lateral viscosity variations beneath Antarctica and their implications on regional rebound motions and seismotectonics. Journal of Geodynamics, 39, 165-181, doi:10.1016/j.jog.2004.08.009, 2005.

Kearey, P., Klepeis, K.A., and Vine, F.J.: Global tectonics (3rd ed.). Wiley–Blackwell, 2009.

Kendall, R.A., Mitrovica, J.X., and Milne, G.A.: On post-glacial sea level–II. Numerical formulation and comparative results on spherically symmetric models. Geophysical Journal International, 161, 679-706, doi:10.1111/j.1365-246X.2005.02553.x, 2005.

Konrad, H., Sasgen, I., Pollard, D., and Klemann, V.: Potential of the solid-Earth response for limiting long-term West Antarctic Ice Sheet retreat in a warming climate. Earth and Planetary Science Letters, 432, 254-264, doi:10.1016/j.epsl.2015.10.008, 2015.

Lambeck, K., Rouby, H., Purcell, A., Sun, Y., and Sambridge, M.: Sea level and global ice volumes from the Last Glacial Maximum to the Holocene. PNAS, 111, 15296-15303, doi:10.1073/pnas.1411762111, 2014.

Larour, E., Seroussi, H., Adhikari, S., Ivins, E., Caron, L., Morlighem, M., and Schlegel, N.: Slowdown in Antarctic mass loss from solid Earth and sea-level feedbacks. Science, 364, doi:10.1126/science.aav7908, 2019.

Laskar, J., Robutel, P., Joutel, F., Gastineau, M., Correia, A.C.M., and Levrard, B.: A long-term numerical solution for the insolation quantities of the Earth. Astronomy & Astrophysics, 428, 261-285, doi:10.1051/0004-6361:20041335, 2004.

Lau, H.C., Mitrovica, J.X., Austermann, J., Crawford, O., Al-Attar, D., and Latychev, K.: Inferences of mantle viscosity based on ice age data sets: Radial structure. J. Geophys. Res. Solid Earth, 121, 6991-7012, doi:10.1111/j.1365-246X.2005.02536.x, 2016.

Le Brocq, A.M., Payne, A.J., and Vieli, A.: An improved Antarctic dataset for high resolution numerical ice sheet models (ALBMAP v1). Earth System Science Data, 2, 247-260, doi:10.5194/essd-2-247-2010, 2010.

800 Le Meur, E., and Huybrechts, P.: A comparison of different ways of dealing with isostasy: examples from modelling the Antarctic Ice Sheet during the last glacial cycle. Annals of Glaciology, 23, 309-317, doi:10.3189/S0260305500013586, 1996.

Martin, M.A., Winkelmann, R., Haseloff, M., Albrecht, T., Bueler, E., Khroulev, C., and Levermann, A.: The Potsdam Parallel Ice Sheet Model (PISM-PIK)-part 2: dynamic equilibrium simulation of the Antarctic Ice Sheet. The Cryosphere, 5, 3, 805 727-740, doi:10.5194/tc-5-727-2011, 2011.

Martin, A.P.: A review of the composition and chemistry of peridotite mantle xenoliths in volcanic rocks from Antarctica and their relevance to petrological and geophysical models for the lithospheric mantle. Geological Society, London, Memoirs, 56, doi:10.1144/M56-2021-26, 2021.

Meredith, M., Sommerkorn, M., Cassotta, S., … Schuur, E.A.G.: Chapter 3: Polar Regions. IPCC SR Ocean and Cryosphere, 810 2019.

Morland, L.W., and Johnson, I.R.: Steady motion of ice sheets. Journal of Glaciology, 25, 229–246, doi:10.3189/S0022143000010467, 1980.

Morland, L.W.: Unconfined ice-shelf flow. Dynamics of the West Antarctic Ice Sheet, 99–116, doi:10.1007/978-94-0093745-1_6, 1987.

815 Nield, G.A., Barletta, V.R., Bordoni, A., ... and Berthier, E.: Rapid bedrock uplift in the Antarctic Peninsula explained by viscoelastic response to recent ice unloading. Earth and Planetary Science Letters, 397, 32-41, doi:10.1016/j.epsl.2014.04.019, 2014.

Nield, G.A., Whitehouse, P.L., van der Wal, W., Blank, B., O'Donnell, J.P., and Stuart, G.W.: The impact of lateral variations in lithospheric thickness on glacial isostatic adjustment in West Antarctica. Geophysical Journal International, 214, 811-820 824, doi:10.1093/gji/ggy158, 2018.

Pan, L., Powell, E.M., Latychev, K., Mitrovica, J.X., Creveling, J.R., Gomez, N., ... and Clark, P.U.: Rapid postglacial rebound amplifies global sea level rise following West Antarctic Ice Sheet collapse. Science Advances, 7, eabf7787, doi:10.1126/sciadv.abf7787, 2021.

Pappa, F., Ebbing, J., Ferraccioli, F., and van der Wal, W.: Modeling satellite gravity gradient data to derive density, 825 temperature, and viscosity structure of the Antarctic lithosphere. Journal of Geophysical Research: Solid Earth, 124, 12053-12076, doi:10.1029/2019JB017997, 2019.

Pattyn, F.: Sea-level response to melting of Antarctic ice shelves on multi-centennial timescales with the fast Elementary Thermomechanical Ice Sheet model (f. ETISh v1. 0). The Cryosphere, 11, 1851-1878, doi:10.5194/tc-11-1851-2017, 2017.

830 Pattyn, F., and Morlighem, M.: The uncertain future of the Antarctic Ice Sheet. Science, 367, 1331-1335, doi:10.1126/science.aaz5487, 2020.

Pelletier, C., Fichefet, T., Goosse, H., Haubner, K., Helsen, S., Huot, P.V., ... and Zipf, L.: PARASO, a circum-Antarctic fully coupled ice-sheet–ocean–sea-ice–atmosphere–land model involving f. ETISh1. 7, NEMO3. 6, LIM3. 6, COSMO5. 0 and CLM4. 5. Geoscientific Model Development, 15, 553-594, doi:10.5194/gmd-15-553-2022, 2022.

835   Peltier, W.R. Ice age paleotopography. Science, 265, 195-201, 1994.

Pollard, D., and DeConto, R.: Modelling West Antarctic Ice Sheet growth and collapse through the past five million years. Nature, 458, 329–332, doi:10.1038/nature07809, 2009.

Pollard, D., Gomez, N., and DeConto, R.M.: Variations of the Antarctic Ice Sheet in a coupled ice sheet-Earth-sea level model: sensitivity to viscoelastic Earth properties. Journal of Geophysical Research: Earth Surface, 122, 2124-2138,
840   doi:10.1002/2017JF004371, 2017.

Powell, E.M., Pan, L., Hoggard, M.J., Latychev, K., Gomez, N., Austermann, J., and Mitrovica, J.X.: The impact of 3-D Earth structure on far-field sea level following interglacial West Antarctic Ice Sheet collapse. Quaternary Science Reviews, 273, 107256, doi:10.1016/j.quascirev.2021.107256, 2021.

Reerink, T.J., Van De Berg, W.J., and Van De Wal, R.S.W.: OBLIMAP 2.0: a fast climate model-ice sheet model coupler
845   including online embeddable mapping routines. Geoscientific Model Development, 9, 4111-4132, doi:10.5194/gmd-9-4111-2016, 2016.

Scheinert, M., Engels, O., Schrama, E.J., van der Wal, W., and Horwath, M.: Geodetic observations for constraining mantle processes in Antarctica. Geological Society, London, Memoirs, 56, doi:10.1144/M56-2021-22, 2021.

Schoof, C.: Ice sheet grounding line dynamics: Steady states, stability, and hysteresis. Journal of Geophysical Research: Earth
850   Surface, 112, doi:10.1029/2006JF000664, 2007.

Shepard, D.: A two-dimensional interpolation function for irregularly-spaced data. Proceedings-1968 ACM National Conference, 517–524, doi:10.1145/800186.810616, 1968.

Shepherd, A., Ivins, E., Rignot, E., Smith, B., Van Den Broeke, M., Velicogna, I., ... and Wouters, B.: Mass balance of the Antarctic Ice Sheet from 1992 to 2017. Nature, 558, 219-222, doi:10.1038/s41586-018-0179-y, 2018.

855   Simon, K. M., James, T. S., and Ivins, E. R.: Ocean loading effects on the prediction of Antarctic glacial isostatic uplift and gravity rates. Journal of Geodesy, 84, 305-317, doi:10.1007/s00190-010-0368-4, 2010.

Spada, G., Barletta, V.R., Klemann, V., Riva, R.E.M., Martinec, Z., Gasperini, P., et al.: A benchmark study for glacial isostatic adjustment codes. Geophysical Journal International, 185, 106–132, doi:10.1111/j.1365-246x.2011.04952.x, 2011.

Van De Wal, R.S.W., De Boer, B., Lourens, L.J., Köhler, P., and Bintanja, R.: Reconstruction of a continuous high-resolution
860   CO2 record over the past 20 million years. Climate of the Past, 7, 1459-1469, doi:10.5194/cp-7-1459-2011, 2011.

Van Den Berg, J., Van De Wal, R. S.W., & Oerlemans, J.: A mass balance model for the Eurasian Ice Sheet for the last 120,000 years. Global and Planetary Change, 61, 194-208, doi:10.1029/2007JB004994, 2008.

Van Der Wal, W., Wu, P., Wang, H., and Sideris, M.G.: Sea levels and uplift rate from composite rheology in glacial isostatic adjustment modeling. Journal of Geodynamics, 50, 38-48, doi:10.1016/j.jog.2010.01.006, 2010.

865   Van Der Wal, W., Barnhoorn, A., Stocchi, P., Gradmann, S., Wu, P., Drury, M., and Vermeersen, B.: Glacial isostatic adjustment model with composite 3-D Earth rheology for Fennoscandia. Geophysical Journal International, 194, 61-77, doi:10.1093/gji/ggt099, 2013.

Van Der Wal, W., Whitehouse, P.L., and Schrama, E.J.O.: Effect of GIA models with 3D composite mantle viscosity on GRACE mass balance estimates for Antarctica. Earth and Planetary Science Letters, 414, 134–143,
870   doi:10.1016/j.epsl.2015.01.001, 2015.

Van Der Wal, W., and IJpelaar, T.: The effect of sediment loading in Fennoscandia and the Barents Sea during the last glacial cycle on glacial isostatic adjustment observations. Solid Earth, 8, 955-968, doi:10.5194/se-8-955-2017, 2017.

Weerdesteijn, M., Hu, H., van der Wal, W., and Riva, R.: The potential of numerical modelling for glaciation-induced true polar wander of the Earth. In Geophysical Research Abstracts, 21, ISSN:1029-7006, 2019.

875   Weihaupt, J.G., Chambers, F.B., van der Hoeven, F.G., and Lorius, C.: Impact crater morphology: The origin of the Mertz and Ninnis Glaciers, Antarctica. Geomorphology, 209, 133-139, doi:10.1016/j.geomorph.2013.11.031, 2014.

Whitehouse, P.L., Bentley, M.J., Milne, G.A., King, M.A., and Thomas, I.D.: A new glacial isostatic adjustment model for Antarctica: calibrated and tested using observations of relative sea-level change and present-day uplift rates. Geophysical Journal International, 190, 1464-1482, doi:10.1111/j.1365-246X.2012.05557.x, 2012.

880   Whitehouse, P.L., Gomez, N., King, M.A., and Wiens, D.A.: Solid Earth change and the evolution of the Antarctic Ice Sheet. Nature communications, 10, 1-14, doi:10.1038/s41467-018-08068-y, 2019.

Wu, P., and Peltier, W. R.: Viscous gravitational relaxation. Geophysical Journal International, 70(2), 435-485, doi: 10.1111/j.1365-246X.1982.tb04976.x, 1982.

Wu, P.: Using commercial finite element packages for the study of Earth deformations, sea levels and the state of stress.
885   Geophysical Journal International, 158, 2, 401–408, doi:10.1111/j.1365-246X.2004.02338.x, 2004.

Yousefi, M., Wan, J., Pan, L., Gomez, N., Latychev, K., Mitrovica, J. X., Pollard, D., and DeConto, R.M.: The influence of the solid Earth on the contribution of marine sections of the Antarctic Ice Sheet to future sea-level change. Geophysical Research Letters, 49, doi:10.1029/2021GL097525, 2022.